A transcriptomics resource reveals a transcriptional transition during ordered sarcomere morphogenesis in flight muscle

Spletter, Maria L ; Barz, Christiane ; Yeroslaviz, Assa ; Zhang, Xu ; Lemke, Sandra B ; Bonnard, Adrien ; Brunner, Erich ; Cardone, Giovanni ; Basler, Konrad ; Habermann, Bianca H ; Schnorrer, Frank

Abstract: Muscles organise pseudo-crystalline arrays of actin, myosin and titin filaments to build force-producing sarcomeres. To study sarcomerogenesis, we have generated a transcriptomics resource of developing flight muscles and identified 40 distinct expression profile clusters. Strikingly, most sarcomeric components group in two clusters, which are strongly induced after all myofibrils have been assembled, indicating a transcriptional transition during myofibrillogenesis. Following myofibril assembly, many short sarcomeres are added to each myofibril. Subsequently, all sarcomeres mature, reaching 1.5 µm diameter and 3.2 µm length and acquiring stretch-sensitivity. The efficient induction of the transcriptional transition during myofibrillogenesis, including the transcriptional boost of sarcomeric components, requires in part the transcriptional regulator Spalt major. As a consequence of Spalt knock-down, sarcomere maturation is defective and fibers fail to gain stretch-sensitivity. Together, this defines an ordered sarcomere morphogenesis process under precise transcriptional control - a concept that may also apply to vertebrate muscle or heart development.

DOI: https://doi.org/10.7554/eLife.34058

A transcriptomics resource reveals a transcriptional transition during ordered sarcomere morphogenesis in flight muscle

Maria L. Spletter[1,2], Christiane Barz[1], Assa Yeroslaviz[3], Xu Zhang[1,4,5], Sandra B. Lemke[1], Adrien Bonnard[4], Erich Brunner[6], Giovanni Cardone[7], Konrad Basler[6], Bianca H. Habermann[3,4], Frank Schnorrer[1,4]

[1] Muscle Dynamics Group, Max Planck Institute of Biochemistry, 82152 Martinsried, Germany

[2] Ludwig-Maximilians-Universität München, Biomedical Center, Physiological Chemistry, 82152 Martinsried, Germany

[3] Computational Biology Group, Max Planck Institute of Biochemistry, 82152 Martinsried, Germany

[4] Aix Marseille University, CNRS, IBDM, 13288 Marseille, France

[5] School of Life Science and Engineering, Foshan University, China

[6] Institute of Molecular Life Sciences, University of Zurich, 8057 Zurich, Switzerland;

[7] Imaging Facility, Max Planck Institute of Biochemistry, 82152 Martinsried, Germany

Correspondence should be addressed to:

frank.schnorrer@univ-amu.fr

maria.spletter@bmc.med.lmu.de

keywords: muscle; sarcomere; myofibril; RNA-Seq; transcription; *Drosophila*

Abstract

Muscles organise pseudo-crystalline arrays of actin, myosin and titin filaments to build force-producing sarcomeres. To study sarcomerogenesis, we have generated a transcriptomics resource of developing *Drosophila* flight muscles and identified 40 distinct expression profile clusters. Strikingly, most sarcomeric components group in two clusters, which are strongly induced after all myofibrils have been assembled, indicating a transcriptional transition during myofibrillogenesis. Following myofibril assembly, many short sarcomeres are added to each myofibril. Subsequently, all sarcomeres mature, reaching 1.5 μm diameter and 3.2 μm length and acquiring stretch-sensitivity. The efficient induction of the transcriptional transition during myofibrillogenesis, including the transcriptional boost of sarcomeric components, requires in part the transcriptional regulator Spalt major. As a consequence of Spalt knock-down, sarcomere maturation is defective and fibers fail to gain stretch-sensitivity. Together, this defines an ordered sarcomere morphogenesis process under precise transcriptional control – a concept that may also apply to vertebrate muscle or heart development.

Introduction

Sarcomeres are the stereotyped force producing mini-machines present in all striated muscles of bilaterians. They are built of three filament types arrayed in a pseudo-crystalline order: actin filaments are cross-linked with their plus ends at the sarcomeric Z-disc and face with their minus ends towards the sarcomere center. In the center, symmetric bipolar muscle myosin filaments, anchored at the M-line, can interact with the actin filaments. Myosin movement towards the actin plus ends thus produces force during sarcomere shortening. Both filament types are permanently linked by a third filament type, the connecting filaments, formed of titin molecules (Gautel and Djinovic-Carugo, 2016; Lange et al., 2006). A remarkable feature of sarcomeres is their stereotyped size, ranging from 3.0 to 3.4 μm in relaxed human skeletal muscle fibers (Ehler and Gautel, 2008; Llewellyn et al., 2008; Regev et al., 2011). Even more remarkable, the length of each bipolar myosin filament is 1.6 μm in all mature sarcomeres of vertebrate muscles, requiring about 300 myosin hexamers to assemble per filament (Gokhin and Fowler, 2013; Tskhovrebova and Trinick, 2003).

Human muscle fibers can be several centimetres in length and both ends of each fiber need to be stably connected to tendons to achieve body movements. As sarcomeres are only a few micrometres in length, many hundreds need to assemble into long linear myofibrils that span from one muscle end to the other and thus enable force transmission from the sarcomeric series to the skeleton (Lemke and Schnorrer, 2017). Thus far, we have a very limited understanding of how sarcomeres initially assemble into long immature myofibrils during muscle development to exactly match the length of the mature muscle fiber (Sparrow and Schöck, 2009). In particular, we would like to

understand how such sarcomeres mature to the very precise stereotyped machines present in mature muscle fibers.

Across evolution, both the pseudo-crystalline regularity of sarcomeres as well as their molecular components are well conserved (Ehler and Gautel, 2008; Vigoreaux, 2006). Thus, *Drosophila* is a valid model to investigate the biogenesis of sarcomeres as well as their maturation. In particular, the large indirect flight muscles (IFMs) that span the entire fly thorax are an ideal model system to investigate mechanisms of myofibrillogenesis. They contain thousands of myofibrils consisting of 3.2 µm long sarcomeres (Schönbauer et al., 2011; Spletter et al., 2015).

Like all *Drosophila* adult muscles, IFMs are formed during pupal development from a pool of undifferentiated myoblasts called adult muscle precursors (AMPs) (Bate et al., 1991). From 8 h after puparium formation (APF), these AMPs either fuse with themselves (for the dorso-ventral flight muscles, DVMs) or with remodelled larval template muscles (for the dorso-longitudinal flight muscles, DLMs) to form myotubes (Dutta et al., 2004; Fernandes et al., 1991). These myotubes develop dynamic leading edges at both ends and initiate attachment to their respective tendon cells at 12 to 16 h APF (Weitkunat et al., 2014). These attachments mature and mechanical tension is built up in the myotubes, followed by the formation of the first immature periodic myofibrils at 30 h APF when the muscle fibers are about 150 µm in length. These immature myofibrils contain the earliest sarcomeres, which are about 1.8 µm in length (Weitkunat et al., 2014). During the remaining 3 days of pupal development, the muscle fibers grow to about 1 mm to fill the entire thorax and sarcomere length increases to a final length of about 3.2 µm in adult flies (Orfanos et al., 2015; Reedy and Beall, 1993).

After myoblasts have fused to myotubes, the flight muscle specific selector gene *spalt major* (*spalt*, *salm*) is turned on in the developing flight muscle myotubes. Spalt major is responsible for the correct fate determination and development of the flight muscles, which includes the fibrillar flight muscle morphology and the stretch-activated muscle contraction mode (Schönbauer et al., 2011; Syme and Josephson, 2002). It does so by controlling the expression of more than 700 flight muscle specific genes or gene isoforms during development (Spletter and Schnorrer, 2014; Spletter et al., 2015). However, how the interplay between all these isoforms instructs the formation of highly regular, pseudo-crystalline sarcomeres in the flight muscle is not understood.

Here, we studied the transcriptional dynamics of flight muscle development in detail. We performed a systematic mRNA-Seq time-course of isolated muscle tissue at 8 time points from the myoblast stage until the mature adult muscle stage, generating a transcriptomics resource of developing flight muscle. Bioinformatic analysis of expression dynamics identified two gene clusters that are strongly enriched for sarcomeric genes. The temporal dynamics of these clusters identified a transcriptional transition that is required for sarcomere morphogenesis. We define sarcomere morphogenesis in three sequential although overlapping phases. First, immature myofibrils assemble simultaneously; second, short sarcomeres are added to each myofibril; and third, all sarcomeres mature to their final length and diameter and acquire stretch-sensitivity. Interestingly, the number of myofibrils remains constant, suggesting that every sarcomere progresses through sarcomere maturation. We show that the flight muscle selector gene *spalt major* contributes to the observed transcriptional transition, suggesting that muscle fiber type-specific transcription is continuously required during

sarcomere formation and maturation. Together, these findings indicate that precise transcriptional control of the sarcomeric components enables their ordered assembly into sarcomeres and their maturation to pseudo-crystalline regularity.

Results

A time-course of indirect flight muscle development

To better understand muscle morphogenesis in general and myofibrillogenesis in particular, we focused on the *Drosophila* indirect flight muscles (IFMs). We hypothesised that major morphological transitions during IFM development may be induced by transcriptional changes, thus we aimed to generate a detailed developmental mRNA-Seq dataset from IFMs. IFMs are built from AMPs that adhere to the hinge region of the wing disc epithelium and are labelled with Gma-GFP under *Him* control (Figure 1A) (Soler and Taylor, 2009). At 16 h APF, many of these myoblasts have fused to larval template muscles to build the dorsal-longitudinal flight muscle (DLM) myotubes, which initiate attachment to their tendons. At this stage, the DLM myotubes of fibers 3 and 4 have a length of about 300 µm (Figure 1B). Fusion ceases at about 24 h APF (Figure 1C) and attachment matures until 32 h APF, coinciding with the strong recruitment of βPS-Integrin and the spectraplakin homolog Shortstop (Shot) to the attachment sites. At this stage the myofibers have built up mechanical tension and compacted to a length of about 150 µm, coinciding with the appearance of long Shot-positive tendon extensions that anchor the muscles within the thorax. This important developmental transition is highlighted by the assembly of immature myofibrils visualised by strong F-actin staining throughout the entire muscle fiber (Figure 1D) (Weitkunat et al., 2014).

After 32 h APF, the myofibers undergo another developmental transition and begin to grow dramatically. They elongate 3-fold to reach a length of about 480 µm by 48 h APF (Figure 1E) and about 590 µm by 56 h APF (Figure 1F). Concomitantly, the

tendon extensions shrink with the myofibers being directly connected to the basal side of the tendon cell epithelium by 72 h APF (Figure 1G). At the end of pupal development (90 h APF), wavy muscle fibers with a length of about 780 µm containing mature myofibrils (Figure 1H) are present within the thorax.

A transcriptomics resource of indirect flight muscle development

To quantify transcriptional dynamics across the entire developmental time-course, we focused on the major developmental transitions and isolated mRNA from dissociated myoblasts of dissected or mass-isolated third instar wing discs and from hand-dissected IFMs at 16 h, 24 h, 30 h, 48 h, 72 h and 90 h APF pupae, and adult flies 1 day after eclosion (Figure 1I). We performed mRNA-Seq using at least two biological replicates for each time point (see Materials and Methods). To identify genes with similar temporal expression profiles, we used Mfuzz (Kumar and Futschik, 2007) to cluster standard normalized read counts from all genes expressed above background (12,495 of 13,322 genes). This allowed us to confidently identify 40 distinct genome-wide clusters (Figure 2-S1), each of which contains a unique gene set ranging from 155 to 703 members (Supplementary File 1). These clusters represent various temporal expression dynamics, with high expression at early (myoblast proliferation and fusion), mid (myotube attachment and myofibril assembly) or late (myofiber growth) myogenesis stages or a combination thereof (Figure 1I, Figure 2-S1). These distinct patterns suggest a precise temporal transcriptional regulation corresponding to observed morphological transition points.

159 To verify the mRNA-Seq and cluster analysis, we selected a number of 'indicator'
160 genes with available antibodies or GFP fusion proteins whose expression correlates with
161 important developmental transitions. Twist (Twi) is a myoblast nuclear marker at larval
162 stages and its expression needs to be down-regulated after myoblast fusion in pupae
163 (Anant et al., 1998). We find *twi* mRNA in Mfuzz cluster 27, with high expression in
164 myoblasts until 16 h APF and a significant down-regulation from 24 h APF, which we
165 were able to verify with antibody stainings (Figure 2A-C). The flight muscle fate selector
166 gene *spalt major* (*salm*) (Schönbauer et al., 2011) and its target, the IFM splicing
167 regulator *arrest* (*aret, bruno*) (Spletter et al., 2015) are members of cluster 26 and 14,
168 respectively. Expression of both clusters is up-regulated after myoblast fusion at 16 h
169 APF, which we were able to verify with antibody stainings (Figure 2D-F, Figure 2-S2A-
170 C). The apparent *salm* mRNA peak at 72 h APF, which does not appear to cause a further
171 protein increase, represents a mere 1.3 fold increase in expression and would need further
172 confirmation as Salm, like many transcription factors, is expressed at low levels. For the
173 initiation of muscle attachment, we selected Kon-tiki (Kon) (Schnorrer et al., 2007;
174 Weitkunat et al., 2014), member of cluster 15, which is transiently up-regulated after
175 myoblast fusion, before it is down-regulated again after 30 h APF. Consistently, we
176 found Kon-GFP present at muscle attachment sites at 30 h APF but not at 72 h APF
177 (Figure 2G-I). A similar expression peak shifted to slightly later time points is found in
178 cluster 34, which contains *β-tubulin 60D* (*βTub60D*) (Leiss et al., 1988). Consistently, we
179 find β-Tub60D-GFP (Sarov et al., 2016) expression in IFMs at 30 h and 48 h but not 72 h
180 APF (Figure 2J-L). After attachment is initiated, the attachments need to mature and be
181 maintained. As expected, we found the essential attachment components βPS-Integrin

(*mys*) and Talin (*rhea*) in clusters that are up-regulated after myoblast fusion until adulthood (clusters 7 and 25, respectively). This is consistent with continuous high protein expression of βPS-Integrin-GFP and Talin-GFP at muscle attachment sites (Figure 2M-O, Figure 2-S2D-F). Taken together, these semi-quantitative protein localisation data nicely validate the temporal mRNA dynamics found in the mRNA-Seq data, confirming our methodology.

A transcriptional transition after 30 h APF

Hierarchical clustering of the core expression profiles from the 40 identified Mfuzz clusters defines 8 temporally ordered groups (Figure 3) that show progressive expression dynamics as muscle development proceeds. A time-dependent shift in gene ontology (GO) term enrichments is apparent between the 8 groups, reflecting the different stages of IFM development. GO-Elite analysis (Zambon et al., 2012) for gene set enrichment identified GO terms related to cell proliferation and development as enriched in the early clusters (such as the *twi* cluster 27 or the *kon* cluster 15), whereas terms related to actin filament dynamics are more enriched in the middle clusters (such as the βPS-Integrin cluster 7 and the Talin cluster 25), reassuring that the clustering approach is valid (Figure 3, Supplementary File 2). Strikingly, the only two clusters that display a strong enrichment for genes important for sarcomere organisation are clusters 13 and 22, both of which are late up-regulated clusters (Figure 3). Members of both clusters just become detectable at 30 h APF (Unc-89/Obscurin-GFP, Act88F-GFP, Mhc-GFP) or even later at 48h APF (Strn-Mlck-GFP, Mf-GFP). In all cases, we could confirm the strong up-regulation from 30 h to 72 h APF in the mRNA-Seq data at the protein level using GFP

205 fusion proteins under endogenous control (Figure 2P-U, Figure 2-S2J-P) (Sarov et al.,
206 2016). We additionally verified the late up-regulation of Flightin (Fln), a member of
207 cluster 3, which is detectable at 72 h but not at 30 h APF (Figure 2-S2G-I).

208 At late stages of flight muscle development, mitochondrial density strongly
209 increases (Clark et al., 2006). Using GO-Elite, we found a strong enrichment for
210 mitochondrial related pathways in four late up-regulated clusters, namely 3, 28, 39 as
211 well as the sarcomere cluster 22 (Figure 3). By comparing the clusters to systematic
212 functional data acquired at all stages of *Drosophila* muscle development (Schnorrer et al.,
213 2010), we find enrichments in clusters throughout the time-course. Interestingly, genes
214 highly expressed in flight muscle compared to other muscle types, identified as '*salm*-
215 core genes' (Spletter et al., 2015), are also enriched in the late clusters, including the
216 mitochondrial enriched clusters 3, 28, 39 and the sarcomere enriched cluster 22 (Figure
217 3). These data highlight the changes in biological process enrichments that parallel
218 expression dynamics, with a particular transition happening during later stages of muscle
219 development after 30 h APF. This corresponds to a time period after immature myofibrils
220 have been assembled, which thus far remained largely unexplored.

221 To examine the temporal expression dynamics in more detail, we performed a
222 principle component analysis (PCA) of the mRNA-Seq time points and Mfuzz clusters
223 and found that the major variance is developmental time, with a notable change after 30 h
224 APF (Figure 4A, Figure 4-S1A). There are a large number of genes being up-regulated as
225 well as down-regulated between 30 h and 48 h and between 48 h and 72 h APF, with
226 major differences between the sets of genes expressed at early (16 h - 30 h APF) versus
227 late (72 h - 90 h APF) stages of development (Figure 4B, Figure 4-S1B). Thus, we

focused our attention on the transcriptional transition between 30 h and 72 h APF, which correlates with major growth of the flight muscle fibers (Figure 1).

A large number of genes are significantly up- or down-regulated from 30 h to 72 h APF, as visualized on a volcano plot displaying $\log_2$ fold changes (FC) (Figure 4C), suggesting a major change in gene expression. In particular, many sarcomeric genes are strongly up-regulated. To identify fine details in expression dynamics, we took all genes significantly up-regulated between 30 h and 72 h APF and performed hierarchical clustering of their DESeq2 normalized counts values (Figure 4D). We noted that many genes are turned on from 30 h to 72 h APF, whereas others are already expressed at 30 h and strongly increase their expression until 72 h (Figure 4D), suggesting a transcriptional transition after 30 h APF. Consistently, we found GO-terms of cell proliferation, cell cycle and Notch signalling down-regulated, whereas actin cytoskeleton, sarcomere, muscle function and mitochondrial related gene sets are strongly up-regulated from 30 h to 72 h APF (Figure 4E). Finally, the genes up-regulated from 30 h to 72 h APF are enriched for sarcomeric proteins and the '*salm* core genes' (Figure 4-S1C, D), and the Mfuzz gene clusters with the most up-regulated members are the mitochondrial and both sarcomeric gene containing clusters 13 and 22 (Figure 4F). Together, these data suggest that in particular expression of the sarcomeric and mitochondrial genes is strongly induced after 30 h APF.

Ordered phases during sarcomere morphogenesis

The strong up-regulation of sarcomeric gene expression after immature myofibrils have been assembled (Figure 1) (Weitkunat et al., 2014) caught our interest and prompted us to

more closely investigate the later stages of myofibrillogenesis during which myofibers grow dramatically (Figure 1). We stained the myofibers with phalloidin to reveal myofibril morphology and with the titin isoform Kettin (an isoform of the *sallimus* gene) to label the developing Z-discs and systematically quantified sarcomere length and myofibril width (see Materials and Methods) (Figure 5A, Supplementary File 3). By measuring the total muscle fiber length, we calculated the total number of sarcomeres per myofibril at a given stage. We found that the sarcomere length and width remain relatively constant at about 2.0 µm and 0.5 µm, respectively until 48 h APF (Figure 5B, C, Supplementary File 3). However, the number of sarcomeres per myofibril dramatically increases from about 100 at 34 h to about 230 at 48 h APF. After 48 h only a few more sarcomeres are added, resulting in about 270 sarcomeres per myofibril at 60 h APF. This number remains constant until the fly ecloses (Figure 5D, Supplementary File 3). Moreover, by analysing fiber cross-sections we found that the growth of the individual myofibril diameter correlates with growth of the entire muscle fiber. Both fiber diameter and myofibril diameter remain constant from 30 h to 48 h APF. After 48 h the myofibril diameter grows nearly 3-fold from 0.46 µm to 1.43 µm in adult flies (Figure 5E-G), while fiber cross-sectional area grows nearly 4-fold from 1,759 μm^2 to 6,970 μm^2. Strikingly, during the entire time period from 30 h APF to adults, the total number of myofibrils per muscle fiber remains constant (about 2,000 per muscle fiber, Figure 5H). Taken together, these quantitative data lead us to propose ordered but somewhat overlapping phases of sarcomere morphogenesis: 1) During the sarcomere assembly phase, about 100 immature sarcomeres self-assemble within each immature myofibril. 2) Many short sarcomeres are added to each myofibril increasing its length. 3) The short sarcomeres grow in length and

thickness to reach the mature pseudo-crystalline pattern. No new myofibrils are built after the initial myofibril assembly phase.

We gained additional evidence to support this ordered myofibrillogenesis model on both the molecular and functional levels. First, the initial assembly versus the later sarcomere maturation complement the transition in gene expression we observe from 30 h to 72 h APF. Using members of the late induced Mfuzz clusters that contain sarcomeric components, we found that indeed a subset of sarcomeric proteins, such as Unc-89/Obscurin and Mhc, are already detectable in a periodic pattern on immature myofibrils at 30 h. By contrast, other important components, including Fln, Myofilin (Mf) and Strn-Mlck, are only incorporated into myofibrils from 48 h APF, showing high levels by 72 h APF (Figure 5-S1). Second, to investigate muscle function, we used Talin-YPet as a muscle attachment marker and quantified the number of spontaneous muscle contractions in intact pupae (see Materials and Methods). Interestingly, we found that immature myofibrils already start to spontaneously contract at 30 h APF. These spontaneous contractions increase in strength and frequency until 48 h APF, but then cease, producing no detectable spontaneous contractions at 72 h APF (Figure 5 I,J, Movie 1). This demonstrates that during the sarcomere assembly phase, immature contractile myofibrils are generated, which then likely acquire stretch-sensitivity as the immature myofibrils mature and thus cease contracting.

Salm contributes to the transcriptional transition after 30 h APF

How does the transcriptional transition of the various sarcomeric components instruct myofibrillogenesis? As the identified sarcomeric clusters 13 and 22 are enriched for

297 '*salm*-core genes' (Spletter et al., 2015) (Figure 3), we chose to investigate gene
298 expression in developing *spalt-major* knock-down (*salmIR*) flight muscles compared to
299 wild type (Supplementary File 4). *salmIR* IFM shows a strong down-regulation in gene
300 expression, notably of mRNAs coding for sarcomeric and mitochondrial components at
301 24 h and 30 h APF, and in particular at 72 h APF (Figure 6A-C, Figure 6-S1A-D). The
302 genes down-regulated in *salmIR* IFM are enriched for GO terms associated with
303 sarcomere assembly, flight behaviour and mitochondrial genes, as well as for the
304 mitochondrial Mfuzz clusters 3, 28, 39 and the sarcomeric Mfuzz clusters 13 and 22
305 (Figure 6-S1E-G). Interestingly, members of cluster 22, which is strongly enriched for
306 sarcomeric and mitochondrial genes, are not only down-regulated at 72 h APF in *salmIR*
307 (Figure 6B) but are also less strongly induced from 30 h to 72 h APF in *salmIR* muscle
308 compared to wild type (Figure 6D), suggesting that *salm* in addition to other factors is
309 indeed required for the strong induction of sarcomeric protein expression after 30 h APF.
310 Salm is expressed shortly after myoblast fusion and constitutive knock-down of
311 *salm* with *Mef2*-GAL4 results in a major shift of muscle fiber fate (Schönbauer et al.,
312 2011), which may indirectly influence transcription after 30 h APF. Hence, we aimed to
313 reduce Salm levels only later in development, to directly address its role during
314 sarcomere maturation. To this end, we knocked-down *salm* with the flight muscle
315 specific driver *Act88F*-GAL4, which is expressed from about 18 h APF and requires *salm*
316 activity for its expression (Bryantsev et al., 2012; Spletter et al., 2015). This strategy
317 enabled us to reduce Salm protein levels at 24 h APF resulting in undetectable Salm
318 levels at 72 h APF (Figure 6-S2). To test if Salm contributes to the transcriptional boost
319 of sarcomeric components after 30 h APF, we performed quantitative imaging using

320 unfixed living flight muscles expressing GFP fusion proteins under endogenous control.
321 We used green fluorescent beads to normalise the GFP intensity between different
322 samples, and could verify the induction of Mhc, Unc-89, Fln and Strn-Mlck on the
323 protein level from 30 h to 72 h APF (Figure 6-S3). While overall sarcomere morphology
324 is not strongly affected in *Act88F>>salmIR* muscles, we found that the levels of Strn-
325 Mlck, Fln and Mhc proteins are strongly reduced at 90 h as compared to wild-type
326 controls (Figure 6D-H). This suggests that *salm* indeed contributes to the transcriptional
327 transition that boosts the expression of a number of sarcomeric proteins after 30 h APF.
328 To investigate the consequences of late *salm* knock-down, we quantified the
329 myofibril and sarcomere morphology from 48 h onwards. The myofibrils display a
330 fibrillar morphology, confirming that the early function of Salm to determine IFM fate
331 was unaffected by our late knock-down. At 72 h APF and more prominently at 90 h APF
332 and in adults, *Act88F>>salmIR* myofibrils showed actin accumulations at broadened Z-
333 discs (Figure 7A-H), which are often a landmark of nemaline myopathies (Sevdali et al.,
334 2013; Wallgren-Pettersson et al., 2011). The myofibril width was not significantly
335 different in these myofibrils (Figure 7I). However, the sarcomeres of *Act88F>>salmIR*
336 muscles displayed a strong defect in sarcomere length growth after 48 h APF (Figure 7J,
337 Supplemental File 3), with sarcomeres only obtaining a length of 2.8 μm in adult flies,
338 demonstrating that Salm in addition to other factors is required for normal sarcomere
339 maturation.
340
341 **Salm function contributes to gain of stretch-activation during sarcomere maturation**

342 Given the defects in sarcomere length and sarcomere gene expression in
343 *Act88F>>salmIR* muscles, we explored the function of these abnormal muscle fibers. As
344 expected, *Act88F>>salmIR* flies are flightless (Figure 7S1A) and we observed rupturing
345 of the adult muscle fibers within 1d after eclosion (Figure 7S1B-G), demonstrating the
346 importance of proper sarcomere maturation to prevent muscle atrophy. Based on our
347 finding that spontaneous flight muscle contractions stop by 72 h APF, we hypothesized
348 that if Salm truly regulates sarcomere maturation, we may see spontaneous contraction
349 defects during development. At 48 h APF, *Act88F>>salmIR* fibers twitch, but less often
350 than and without the double twitches observed in control fibers (Figure 7K,L,O; Movie
351 2). Strikingly, at 72 h APF *salmIR* fibers fail to stop contracting and moreover show
352 frequent and uncoordinated spontaneous contractions in which different myofibril
353 bundles of the same fiber twitch at different times (Figure 7M-O, Movie 3),
354 demonstrating that sarcomere maturation is indeed disrupted, with the likely consequence
355 that myofibrils fail to acquire normal stretch-activation sensitivity.

356 To directly test the function of a sarcomeric component during the sarcomere
357 maturation phase, we investigated the role of the prominently induced Salm target Strn-
358 Mlck. Strn-Mlck is only expressed after 30 h APF and is largely incorporated during
359 sarcomere maturation (Figure 5S1E, Figure 6S3E), and thus is also a bone-fide example
360 of a gene regulated during the transcriptional transition. In *Strn-Mlck* mutants, sarcomere
361 and myofibril morphology, including myofibril width, is initially normal. However, at 80
362 h APF the sarcomeres overgrow, consistently reaching lengths of more than 3.5 μm and
363 resulting in slightly longer muscle fibers at 80 h APF (Figure 8). After overgrowing,
364 sarcomeres appear to hyper-contract resulting in short, thick sarcomeres in 1-day-old

365 adults (Figure 8E, J, K, L). Like *Act88F>>salmIR* flies, *Strn-Mlck* mutant adults are
366 flightless (Figure 7S1A) and display ruptured fibers during the first days of life (Figure
367 7S1K-M) (Spletter et al., 2015). Together, these data demonstrate that sarcomere
368 maturation must be precisely controlled at the transcriptional level to enable the precise
369 growth of sarcomeres to their final mature size. This ensures the lifelong function of the
370 contractile apparatus of muscle fibers.
371
372

Discussion

A developmental muscle transcriptomics resource

In this study, we generated a systematic developmental transcriptomics resource from *Drosophila* flight muscle. The resource quantifies the transcriptional dynamics across all the major stages of muscle development over five days, starting with stem cell-like myoblasts and attaching myotubes to fully differentiated, stretch-activatable muscle fibers. We have specifically focused on the transcriptional regulation of sarcomere and myofibril morphogenesis; however, the data we provide cover all other expected dynamics, such as mitochondrial biogenesis, T-tubule morphogenesis, neuromuscular junction formation, tracheal invagination, *etc*. Thus, together with the available systematic functional data of *Drosophila* muscle development (Schnorrer et al., 2010), our data should be a versatile resource for the muscle community. It nicely complements existing systematic data from vertebrate muscle, which thus far are largely restricted to postnatal stages (Brinegar et al., 2017; Drexler et al., 2012; Lang et al., 2017; Zheng et al., 2009). Furthermore, *Drosophila* flight muscle contains a single muscle fiber type, in contrast to the mixed fiber types found in mammals (Schiaffino and Reggiani, 2011; Spletter and Schnorrer, 2014). Hence, in this model the transcriptional dynamics of a single fiber type muscle can be followed with unprecedented precision.

A transcriptional transition correlating with ordered sarcomere morphogenesis

Earlier work has shown that the flight muscle myotubes first attach to tendon cells and then build-up mechanical tension. This tension triggers the simultaneous assembly of immature myofibrils, converting the myotube to an early myofiber (Weitkunat et al.,

2014). This suggested a tension-driven self-organisation mechanism of myofibrillogenesis (Lemke and Schnorrer, 2017). Here we discovered that myofibrillogenesis is not only regulated mechanically, but to a large extent also transcriptionally. This enabled us to extend our model for ordered myofibrillogenesis also to later developmental stages and to define three sequential although somewhat overlapping phases (Figure 9). During the sarcomere self-assembly phase at about 30 h APF, a large number of genes coding for sarcomeric proteins, including Mhc, Act88F and Unc-89/Obscurin, become up-regulated to enable the self-organization of short, immature sarcomeres within thin, immature myofibrils. Strikingly, all of the about 2000 myofibrils assemble during this phase.

This is followed by a sarcomere addition phase during which a transcriptional transition is initiated and the expression of the sarcomeric proteins increases. Concomitantly, the muscle fibers grow in length by addition of new sarcomeres to all the immature myofibrils, increasing the sarcomere number from about 80 to 230 per fibril at 48 h APF. These sarcomeres are contractile, but remain short and thin (Figure 9).

After the transcriptional transition, myofibrillogenesis enters the final sarcomere maturation phase. Proteins present in immature myofibrils like Mhc, Act88F and Unc-89/Obscurin are expressed to even higher levels, and additional, often flight-muscle specific proteins like Mf, Fln and the titin-related isoform Strn-Mlck, begin to be expressed at high levels and are incorporated into the maturing sarcomeres. This facilitates a dramatic growth of all immature sarcomeres in length and particularly in diameter with all 2000 myofibrils reaching a pseudo-crystalline regularity within about two days of development (Figure 9). Importantly, these matured sarcomeres no longer

contract spontaneously, likely because they acquired the stretch-activated mechanism of contraction described for mature *Drosophila* flight muscles (Bullard and Pastore, 2011; Josephson, 2006).

Our ordered sarcomere morphogenesis model is strongly supported by the observation that the number of myofibrils remains largely constant during the entire sarcomere morphogenesis period, suggesting that in flight muscles no new myofibrils are added after the initial assembly of immature myofibrils at about 30 h APF. As all sarcomeres are present shortly after 48 h APF, they all need to mature simultaneously to achieve their final pseudo-crystalline regularity.

Our model is further supported by previous studies. We and others found that immature myofibrils have a width of about 0.5 µm (Weitkunat et al., 2014), which corresponds to about 4 thick filaments across each myofibril at the EM level at 42 h APF (at 22ºC) (Reedy and Beall, 1993). This 'core' myofibril structure built until 48 h APF, when most sarcomeres have formed, is expanded dramatically after 48 h APF, reaching a mature width of 1.5 µm, corresponding to about 35 thick filaments across each myofibril at the EM-level (Reedy and Beall, 1993). Recent data showed that the 'core' myofibril structure built until 48 h APF contains already highly ordered actin filaments, which gain even higher order to reach their pseudo-crystalline regularity at 90 h APF (Loison et al., 2018). In total, each adult myofibril contains around 800 thick filaments per sarcomere (Gajewski and Schulz, 2010). The 'core' myofibril structure was also revealed by the preferential recruitment of over-expressed actin isoforms (Roper et al., 2005) and more importantly, by selective incorporation of a particular Mhc isoform that is only expressed at mid-stages of flight muscle development (Orfanos and Sparrow, 2013). This Mhc

isoform expression switch coincides with the global transition in sarcomeric gene expression between the sarcomere assembly and the sarcomere maturation phases that we defined here. It also fits with the recent discovery that the formin family member Fhos is selectively required for actin filament elongation and recruitment of new actin filaments and thus myofibril diameter growth after 48 h APF (Shwartz et al., 2016). Expression of Fhos is also induced after 30 h APF. Fhos is a member of Mfuzz Cluster 28, another strongly induced cluster, underscoring the general relevance of the transcriptional transition for ordered sarcomerogenesis.

Regulated active sarcomere contractions

Mature indirect flight muscles employ a stretch-activated mechanism of muscle contraction, thus Ca^{2+} is not sufficient to trigger muscle contractions without additional mechanical stretch (Bullard and Pastore, 2011; Josephson, 2006). This is different to cross-striated body muscles of flies or mammals that contract synchronously with Ca^{2+} influx. Hence, it is intriguing that immature flight muscle myofibrils do in fact contract spontaneously, with the contraction frequencies and intensities increasing until 48 h APF. It was recently proposed in *Drosophila* cross-striated abdominal muscles and in the developing cross-striated zebrafish muscles that spontaneous contractions are important for the proper formation of the cross-striated pattern (Mazelet et al., 2016; Weitkunat et al., 2017). A similar role for contractions was found in C2C12 cells by stimulating the contractions optogenetically (Asano et al., 2015). This shows that spontaneous contractions are a necessary general feature for the assembly of cross-striated muscle fibers across species.

However, flight muscles are not cross-striated in the classical sense, but have a fibrillar organisation in which each myofibril remains isolated and is not aligned with its neighbouring myofibrils (Figure 5) (Josephson, 2006; Schönbauer et al., 2011). We can only speculate about the mechanism that prevents alignment of the myofibrils in the flight muscles, but it is likely related to their stretch-activated contraction mechanism. This mechanism prevents spontaneous twitching due to increased Ca^{2+} levels, because it additionally requires mechanical activation that can only occur during flight in the adult. Thus, flight muscle sarcomeres not only grow and mature their sarcomere structure, they also gain their stretch-activatability.

Continuous maintenance of muscle type-specific fate

We identified an important transition in gene expression between the early sarcomere assembly and the late sarcomere maturation phases. Similar large scale transcriptome changes have also been observed during postnatal stages of mouse (Brinegar et al., 2017), chicken (Zheng et al., 2009) and pig (Zhao et al., 2015) skeletal muscle development or during regeneration after injury in fish (Montfort et al., 2016) and mouse muscles (Warren et al., 2007), indicating that muscle maturation generally correlates with large scale transcriptional changes.

It is well established that general myogenic transcription factors, in particular Mef2, are continuously required in muscles for their normal differentiation (Sandmann et al., 2006; Soler et al., 2012). Mef2 regulates a suit of sarcomeric proteins in fly, fish and mouse muscle important for correct sarcomere assembly and maturation (Hinits and Hughes, 2007; Kelly et al., 2002; Potthoff et al., 2007; Stronach et al., 1999). In

488 *Drosophila*, Mef2 cooperates with tissue-specific factors, such as CF2, to induce and
489 fine-tune expression of structural genes (Gajewski and Schulz, 2010; Mas et al., 2008;
490 Tanaka et al., 2008). General transcriptional regulators, such as E2F, further contribute to
491 high levels of muscle gene expression during myofibrillogenesis, in part through
492 regulation of Mef2 itself (Zappia and Frolov, 2016). However, it is less clear if muscle
493 type-specific identity genes are continuously required to execute muscle type-specific
494 fate. Spalt major (Salm) is expressed after myoblast fusion in flight muscle myotubes and
495 is required for all flight muscle type-specific gene expression: in its absence the fibrillar
496 flight muscle is converted to tubular cross-striated muscle (Schönbauer et al., 2011;
497 Spletter et al., 2015). Here we demonstrated that Salm is continuously required for
498 correct sarcomere morphogenesis, as late *salm* knock-down leads to defects in sarcomere
499 growth during the late sarcomere maturation phase, causing severe muscle atrophy in
500 adults. It may possibly do so by modifying the cooperation between Mef2 and E2F or by
501 changing chromatin states, as vertebrate spalt homologs are recently discussed as
502 epigenetic regulators (Yang, 2018; Zhang et al., 2015). However, Salm cannot be solely
503 responsible for the transcriptional transition after 30 h APF, as the transition still partially
504 occurs in its absence.
505
506 **Ordered sarcomere morphogenesis – a general mechanism?**
507 Here we defined ordered phases of sarcomere morphogenesis in *Drosophila* flight
508 muscles. Is this a general concept for sarcomere morphogenesis? Reviewing the
509 literature, one finds that in other *Drosophila* muscle types which display a tubular cross-
510 striated myofibril organisation, such as the fly abdominal muscles, the striated

sarcomeres also first assemble and then grow in length (Pérez-Moreno et al., 2014; Weitkunat et al., 2017), suggesting a conserved mechanism. In developing zebrafish skeletal muscles, young myofibers present in younger somites show a short sarcomere length of about 1.2 µm, which increases to about 2.3 µm when somites and muscle fibers mature (Sanger et al., 2017; 2009). Interestingly, sarcomere length as well as thick filament length increase simultaneously during fish muscle maturation, indicating that as in flight muscles, the length of all sarcomeres in one large muscle fiber is homogenous at a given time (Sanger et al., 2009). Similar results were obtained in mouse cardiomyocytes measuring myosin filament length at young (2 somite) and older (13 somite) stages (Du et al., 2008) and even in human cardiomyocytes, in which myofibrils increase nearly threefold in width and become notably more organized and contractile from 52 to 127 days of gestation (Racca et al., 2016). These data suggest that sarcomeres generally may go through a series of ordered but overlapping developmental phases.

Interestingly, these changes in sarcomere morphology correlate with a switch in myosin heavy chain isoform expression changing from embryonic to neonatal to adult during skeletal muscle development (Schiaffino et al., 2015). Importantly, mutations in embryonic myosin (MYH3 in humans) result in severe congenital disorders characterised by multiple facial and limb contractures (Toydemir et al., 2006). As a similar ordered expression of myosin isoforms is also found during muscle regeneration after injury in adults (Ciciliot and Schiaffino, 2010; Schiaffino et al., 2015), we hypothesize that our sequential sarcomere morphogenesis model may also be applicable to vertebrate skeletal and possibly heart muscles. It will be a future challenge to identify possible feedback mechanisms that indicate the successful end of the sarcomere assembly phase or a

534 possible re-entry into the sarcomere assembly phase during muscle regeneration or
535 exercise induced muscle fiber growth. It is enticing to speculate that the assembling
536 cytoskeleton itself would measure its assembly status and provide a mechanical feedback
537 signal to modify the activity of muscle-specific transcription factors.
538
539

Materials and Methods

Key Resource Table

Reagent type (species) or resource	Designation	Source or reference	Identifiers	Additional information
gene (*Drosophila melanogaster*)	spalt major; salm	NA	FLYB:FBgn0261648	
gene (*D. melanogaster*)	Stretchin-Mlck; Strn-Mlck	NA	FLYB:FBgn0265045	
genetic reagent (*D. melanogaster*)	w[1118]	Bloomington	BDSC:3605; FLYB:FBst0003605; RRID:BDSC_3605	
genetic reagent (*D. melanogaster*)	salmIR	PMID: 22094701	VDRC:13302; FLYB:FBst0450930	Flybase symbol: VDRC:v13302
genetic reagent (*D. melanogaster*)	KK101052	PMID: 17625558	VDRC:101052	
genetic reagent (*D. melanogaster*)	Act88F-GAL4	PMID: 22008792		Source: Richard Cripps
genetic reagent (*D. melanogaster*)	Strn-Mlck-MiMIC	Bloomington	FLYB:FBal0264439	Flybase symbol:Strn-MlckMI02893
genetic reagent (*D. melanogaster*)	Strn-Mlck-IR	PMID: 21460824	BDSC:31891; FLYB:FBti0130299; RRID:BDSC_31891	Flybase symbol:P{TRiP.JF02170}attP2
genetic reagent (*D. melanogaster*)	Strn-Mlck-GFP, Isoform R	PMID: 25532219		Symbol: Strn4;
genetic reagent (*D. melanogaster*)	Mhc-GFP	PMID: 26896675	VDRC:318471	Symbol: fTRG500;
genetic reagent (*D. melanogaster*)	Mf-GFP	PMID: 26896675	VDRC:318132	Symbol: fTRG501;
genetic reagent (*D. melanogaster*)	Rhea-GFP	PMID: 26896675	VDRC:318486	Symbol: fTRG587;
genetic reagent (*D. melanogaster*)	Fln-GFP	PMID: 26896675	VDRC:318238	Symbol: fTRG876;
genetic reagent (*D. melanogaster*)	mys-GFP	PMID: 26896675	VDRC:318285	Symbol: fTRG932;
genetic reagent (*D. melanogaster*)	βTub60D-GFP	PMID: 26896675	VDRC:318309	Symbol: fTRG958;
genetic reagent (*D. melanogaster*)	unc-89-GFP	PMID: 26896675	VDRC:318326	Symbol: fTRG1046;
genetic reagent (*D. melanogaster*)	Act88F-GFP	PMID: 26896675	VDRC:318362	Symbol:fTRG10028;
genetic reagent (*D. melanogaster*)	Him-nuc-eGFP	PMID: 19324085		Source: Michael V. Taylor
genetic reagent (*D. melanogaster*)	Him-Gal4	this paper		
genetic reagent (*D. melanogaster*)	UAS-BBM	PMID: 22446736		
genetic reagent (*D. melanogaster*)	Him-Gma-GFP	this paper		
genetic reagent (*D. melanogaster*)	rhea-Ypet	this paper		
genetic reagent (*D. melanogaster*)	kon-GFP	this paper		
genetic reagent (*D. melanogaster*)	Mef2-GAL4	Bloomington	BDSC:27390; RRID:BDSC_27390	
genetic reagent (*D. melanogaster*)	UAS-GFP-Gma	PMID: 12324971		Source:Don Kiehart; Description
antibody	guinea pig anti-Shot	PMID: 9832554		(1:500); Source: Talila Volk
antibody	rat anti-Kettin (MAC155/Klg16)	Babraham Bioscience Technologies	Babraham:MAC_155(P6689)	(1:50)
antibody	rabbit anti-GFP (ab290)	Abcam	Abcam:ab290	(1:1000)
antibody	rat anti-Bruno	PMID: 12591598		(1:500); Source: Anne Ephrussi
antibody	rabbit anti-Salm	PMID: 7905822		(1:50); Source: Reinhard Schuh

antibody	mouse anti-βPS-integrin (CF.6G11)	Developmental Studies Hybridoma Bank	DSHB:CF.6G11	(1:500)
antibody	rabbit anti-Twi	PMID: 2688897		(1:1000); Source: Siegfried Roth
antibody	rabbit anti-Fln	PMID: 11134077		(1:50); Source: Jim Vigoreaux
commercial assay or kit	fluorescent beads	ThermoFisher (Molecular Probes)		OrderID: InSpeckTM Green Kit I-7219
commercial assay or kit	Dynabeads	Invitrogen		OrderID: #610.06
commercial assay or kit	Superscript III First-Strand Synthesis System	Invitrogen		OrderID: #18080-051
chemical compound, drug	Fluoroshield with DAPI	Sigma		OrderID: #F6057
chemical compound, drug	Vectashield with DAPI	Biozol		OrderID: VEC-H-1200
chemical compound, drug	Tissue-Tek O.C.T.	Weckert Labotechnik		OrderID: 4583; Sakura Finetek
chemical compound, drug	TriPure reagent	Roche		OrderID: #11667157001
software, algorithm	Fiji (Image J)	PMID: 22743772		
software, algorithm	MyofibrilJ	this paper	1dbb0d4	Source: https://imagej.net/MyofibrilJ
software, algorithm	STAR	PMID: 23104886		
software, algorithm	SAMtools	PMID: 19505943		
software, algorithm	featureCounts	PMID: 24227677		
software, algorithm	DESeq2	PMID: 25516281		
software, algorithm	R	R Project for Statistical Computing	RRID:SCR_001905	
software, algorithm	ComplexHeatmap	PMID: 27207943		
software, algorithm	corrplot	GitHub		Source: https://github.com/taiyun/corrplot
software, algorithm	VennDiagram	PMID: 21269502		
software, algorithm	plyr	DOI: 10.18637/jss.v040.i01		
software, algorithm	reshape2	DOI: 10.18637/jss.v021.i12		
software, algorithm	ggplot2	ISBN:978-0-387-98140-6		
software, algorithm	RColorBrewer	Author: Erich Neuwirth;		Source: https://cran.r-project.org/web/packages/RColorBrewer/index.html
software, algorithm	Mfuzz	PMID: 16078370		
software, algorithm	GO-Elite	PMID: 22743224		

Fly Strains

Fly stocks were maintained using standard culture conditions. Characterization of normal IFM sarcomere and fiber growth was performed in w^{1118} grown at 27°C. *salm* RNAi was performed with previously characterized GD3029 (referred to as *salmIR)* and KK181052 (Schönbauer et al., 2011) from VDRC (http://stockcenter.vdrc.at) (Dietzl et al., 2007) at 25°C using *Act88F*-GAL4 to induce knock-down after 24 h APF. *Act88F*-GAL4 x w^{1118}

549 served as control. The *Strn-Mlck-MiMIC* insertion MI02893 into IFM-specific IsoR
550 (Bloomington stock 37038) and TRiP hairpin JF02170 were obtained from Bloomington
551 (Ni et al., 2011). The *salm*-EGFP line was used to sort wing discs (Marty et al., 2014).
552 Tagged genomic fosmid reporter fly lines include *strn4* (*Strn-Mlck-GFP*, Isoform R)
553 (Spletter et al., 2015), fTRG500 (*Mhc-GFP*, Isoforms K, L, M), fTRG501 (*Mf-GFP*,
554 Isoforms A, G, N), fTRG587 (*Rhea-GFP*, Isoforms B, E, F, G), fTRG876 (*Fln-GFP*),
555 fTRG932 (*mys-GFP*), fTRG958 (*βTub60D-GFP*), fTRG1046 (*unc-89-GFP*), and
556 fTRG10028 (*Act88F-GFP*) (Sarov et al., 2016).

557 To label myoblasts, we utilized the enhancer for *Holes-in-muscle* (*Him*), which is
558 expressed in dividing myoblasts and promotes the progenitor fate. *Him-nuc-eGFP* flies
559 were a gift of M. Taylor (Soler and Taylor, 2009). *Him*-GAL4 flies were created by
560 cloning an EcoRI to SacII fragment of the *Him* enhancer (Liotta et al., 2007) upstream of
561 GAL4 into pStinger. UAS-BBM (UAS-palmCherry) (Förster and Luschnig, 2012) was
562 driven with *Him*-GAL4 to label myoblasts. *Him*-Gma-GFP flies were created by PCR
563 amplifying Gma-GFP with AscI and PacI overhangs and then cloning downstream of the
564 Him enhancer in pStinger to generate a gypsy insulator-Him^{enh}-Gma-GFP-SV40-gypsy
565 insulator cassette.

566 The *rhea-YPet* line used to label muscle ends for live imaging of twitch events
567 was generated by CRISPR-mediated gene editing at the endogenous locus (S.B.L & F.S.,
568 details will be published elsewhere). The *kon-GFP* line was generated by inserting GFP
569 into the *kon* locus after its transmembrane domain using the genomic fosmid
570 FlyFos021621, which was integrated using Φ-C31 into VK00033 (I. Ferreira and F.S.,
571 details will be published elsewhere).

572

573 **Flight tests**

574 Flight tests were performed as previously described (Schnorrer et al., 2010). *Act88F-*
575 GAL4 crosses were kept at 25°C, as higher temperatures negatively impacted flight
576 ability, because of the very high GAL4 expression levels in this strain. Adult males were
577 collected on CO_2 and recovered at least 24 h at 25°C before testing. Flies were introduced
578 into the top of a 1 m long cylinder divided into 5 zones. Those that landed in the top two
579 zones were considered 'normal fliers', those in the next two zones 'weak fliers' and those
580 that fell to the bottom of the cylinder 'flightless'.

581

582 **Immuno-staining**

583 Wing-discs were dissected from 3rd instar wandering larvae in 1x PBS and fixed in 4%
584 PFA in PBS-T. Discs were stained as described below for anti-GFP. Adult and pupal
585 flight muscles were dissected and stained as previously described (Weitkunat and
586 Schnorrer, 2014). Briefly, early pupae (16 h - 60 h APF) were freed from the pupal case,
587 fixed for 20 min. in 4% PFA in relaxing solution and washed in 0.5% PBS-Triton-X100
588 (PBS-T). 72 h APF and older samples were cut sagittally with a microtome blade. All
589 samples were blocked for at least 1 hour at RT in 5% normal goat serum in PBS-T and
590 stained with primary antibodies overnight at 4°C. Primary antibodies include: guinea pig
591 anti-Shot 1:500 (gift of T. Volk), rat anti-Kettin 1:50 (MAC155/Klg16, Babraham
592 Institute), rabbit anti-GFP 1:1000 (ab290, Abcam), rat anti-Bruno 1:500 (Filardo and
593 Ephrussi, 2003), rabbit anti-Salm 1:50 (Kühnlein et al., 1994), mouse anti-βPS-integrin
594 1:500 (CF.6G11, DSHB), rabbit anti-Twi 1:1000 (gift of Siegfried Roth) and rabbit anti-

595 Fln 1:50 (Reedy et al., 2000)(gift of Jim Vigoreaux). Samples were washed three times
596 in 0.5% PBS-T and incubated overnight at 4°C with secondary conjugated antibodies
597 (1:500) from Invitrogen (Molecular Probes) including: Alexa488 goat anti-guinea pig
598 IgG, Alexa488 donkey anti-rat IgG, Alexa488 goat anti-mouse IgG, Alexa488 goat anti-
599 rabbit IgG, rhodamine-phalloidin, Alexa568 goat anti-rabbit IgG and Alexa633 goat anti-
600 mouse IgG. Samples were washed three times in 0.5% PBS-T and mounted in
601 Vectashield containing DAPI.
602
603 **Cryosections**
604 Head, wings and abdomen were removed from one day old w^{1118} flies and thoraxes were
605 fixed overnight at 4°C in 4% PFA. For 30 - 90 h APF samples, pupae were freed from the
606 pupal case, poked 3-5 times with an insect pin in the abdomen and fixed overnight at 4°C
607 in 4% PFA. Thoraxes or pupae were then sunk in 30% sucrose in 0.5% PBS-T overnight
608 at 4°C on a nutator. Thoraxes or pupae were embedded in Tissue-Tek O.C.T. (Sakura
609 Finetek) in plastic moulds (#4566, Sakura Finetek) and frozen on dry ice. Blocks were
610 sectioned at 30 μm on a cryostat (Microm vacutome). Sections were collected on glass
611 slides coated with 1% gelatin + 0.44 μM chromium potassium sulfate dodecahydrate to
612 facilitate tissue adherence. Slides were post-fixed for 1 min. in 4% PFA in 0.5% PBS-T at
613 RT, washed in 0.5% PBS-T, incubated with rhodamine-phalloidin for 2 hours at RT,
614 washed three times in 0.5% PBS-T and mounted in Fluoroshield with DAPI (#F6057,
615 Sigma).
616
617 **Microscopy and image analysis**

618 Images were acquired with a Zeiss LSM 780 confocal microscope equipped with an α
619 Plan-APOCHROMAT 100x oil immersion objective lens (NA 1.46). To compare if
620 indicator protein expression replicates the mRNA-Seq expression dynamics, we imaged
621 three time points from each expression profile with the same confocal settings. Laser gain
622 and pinhole settings were set on the brightest sample and reused on remaining time points
623 in the same imaging session. All samples were additionally stained with the same
624 antibody mix on the same day and if possible in the same tube. Images were processed
625 with Fiji (Schindelin et al., 2012) and Photoshop, and displayed using the 'Fire' look-up
626 table.

627 Fiber length and fiber cross-sectional area were measured with freehand drawing
628 tools in Fiji based on rhodamine-phalloidin staining. Sarcomere length, myofibril width,
629 and myofibril diameter were measured automatically using a custom Fiji plug-in,
630 MyofibrilJ, available from https://imagej.net/MyofibrilJ and code from
631 https://github.com/giocard/MyofibrilJ (Cardone, 2018). All measurements are based on
632 rhodamine-phalloidin staining, except 34 h APF sarcomere lengths, which are based on
633 both rhodamine-phalloidin and Unc-89-GFP staining. 'Sarcomeres per fibril' was
634 calculated as average individual fiber length divided by sarcomere length for fiber 3 or 4.
635 'Fibrils per fiber' was calculated as average number of fibrils per unit area multiplied by
636 individual fiber cross sectional area.

637 For determining myofibril diameter, samples were imaged using a 3x optical
638 zoom (50 nm pixel size). At least 20 cross-section images from different fibers for >10
639 flies were acquired for each time point. The number of fibrils per section and fibril
640 diameter were determined with the tool 'analyze myofibrils crosswise' from MyofibrilJ

641 (https://imagej.net/MyofibrilJ). In this tool, an initial estimate of the diameter is obtained
642 by finding the first minimum in the radial average profile of the autocorrelation
643 (Goodman, 1968) of the image. This estimate is used to calibrate the optimal crop area
644 around all the cross-sections in the image, their position previously detected by finding
645 the local intensity peaks. All of the detected cross-sections are then combined to obtain a
646 noise-free average representation of the fibril section. Finally, the diameter is calculated
647 by examining the radial profile of the average and measuring the full width where the
648 intensity is 26% of the maximum range.

649 For determining sarcomere length and myofibril width, for each experiment
650 between 10 and 25 images were acquired from more than 10 individual flies. From each
651 image, 9 non-overlapping regions of interest were selected, which were rotated to orient
652 fibrils horizontally, when necessary. The tool 'analyze myofibrils lengthwise' from
653 MyofibrilJ reports the sarcomere length (indicated as repeat) and myofibril width
654 (indicated as thickness). Because of the periodic nature of sarcomere organization, their
655 length is estimated by means of Fourier analysis, identifying the position of the peaks on
656 the horizontal axis of the Fourier transformed imaged. Quality of the estimate was
657 evaluated by visual inspection of the Fourier transformed image, overlaid with the peaks
658 detected, as generated by the plug-in. Myofibrils width is estimated from the position of
659 the first minimum in the vertical intensity profile of the autocorrelation of the image.

660 Live imaging of developmental spontaneous contractions was performed on a
661 Leica SP5 confocal microscope. Prior to imaging, a window was cut in the pupal case,
662 and pupae were mounted in slotted slides as previously described (Lemke and Schnorrer,
663 2018; Weitkunat and Schnorrer, 2014). At the specified developmental time point, IFMs

were recorded every 0.65 seconds for 5 min. General movement within the thorax was distinguished from IFM-specific contraction, and each sample was scored for the number of single or double contractions observed per 5 minute time window. Data were recorded in Excel and ANOVA was performed in GraphPad Prism to determine significant differences. Movies were assembled in Fiji (Image J), cropped and edited for length to highlight a selected twitch event.

Quantitative imaging of fosmid reporter intensity was performed at 30 h APF, 48 h APF, 72 h APF, 90 h APF and in 1 day adult in live IFM by normalizing to fluorescent beads (ThermoFisher (Molecular Probes), InSpeck™ Green Kit I-7219). IFMs were dissected from 5 flies, mounted with fluorescent microspheres (0.3% or 1% relative intensity, depending on the reporter intensity) in the supplied mounting medium and immediately imaged (within 20 minutes). Intensity measurements were obtained at 40x for at least 10 flies in regions where both IFM and at least 3 beads were visible. Control *Act88F-GAL4;; fosmid-GFP* x w^{1118} and *Act88F*-GAL4*;; fosmid-GFP* x *salmIR* (fosmids used included *Strn-Mlck-GFP, Mhc-GFP, Fln-GFP*, and *Unc-89-GFP*) were imaged in the same imaging session. Relative fluorescence fiber to beads was calculated for each image in Fiji by averaging intensity for 3 fiber ROIs and 3 bead ROIs. Data were recorded in Excel and Student's t-test for significance and plotting were performed in GraphPad Prism.

mRNA-Seq

We previously published mRNA-Seq analysis of dissected IFMs from *Mef2*-GAL4, UAS-GFP-Gma x w^{1118} at 30 h APF, 72 h APF and 1d adult, and *Mef2-GAL4, UAS-GFP-*

687 *Gma* x *salmIR* in 1d adult (Spletter et al., 2015). We expanded this analysis in the present
688 study to include myoblasts from 3rd instar larval wing discs (see below) and dissected
689 IFMs from *Mef2*-GAL4, UAS-GFP-Gma x w^{1118} at 16 h, 24 h, 30 h, 48 h, 72 h, 90 h APF
690 and from 1 day adults as well as IFMs from *Mef2*-GAL4, UAS-GFP-Gma x *salmIR* flies
691 at 24 h, 30 h, 72 h APF and from 1 day adults. IFMs were dissected from groups of 15
692 flies in 30 min to minimize changes to the transcriptome, spun down in PBS for 5 min at
693 7500 rpm and immediately frozen in 100 µl TriPure reagent (#11667157001, Roche) on
694 dry ice. RNA was isolated after combining IFMs from 150-200 flies, with biological
695 duplicates or triplicates for each time point.

696 Poly(A)+ mRNA was purified using Dynabeads (#610.06, Invitrogen) and
697 integrity was verified on a Bioanalyzer. mRNA was then fragmented by heating to 94°C
698 for 210 sec in fragmentation buffer (40 mM TrisOAc, 100 mM KOAc, 30 mM $MgOAc_2$).
699 First-strand cDNA synthesis was performed with the Superscript III First-Strand
700 Synthesis System (#18080-051, Invitrogen) using random hexamers. The second strand
701 was synthesized with dUTP and submitted to the Vienna Biocenter Core Facilities
702 (VBCF, http://www.vbcf.ac.at) for stranded library preparation according to standard
703 Illumina protocols and sequenced as SR100 on an Illumina HiSeq2500. Libraries were
704 multiplexed two to four per lane using TrueSeq adaptors.
705
706 **Wing disc sorting and myoblast isolation**
707 To perform mRNA-Seq on fusion competent myoblasts that will form the IFMs, we first
708 dissected wing discs from wandering 3rd instar larvae and manually cut the hinge away
709 from the wing pouch. mRNA was isolated in TriPure reagent and sequenced as described

above. We estimate this sample (Myo1) is ~50% myoblast, as the myoblasts form a nearly uniform layer over the underlying epithelial monolayer. To obtain a purer myoblast sample, we performed large-scale imaginal disc sorting followed by dissociation. We used particle sorting to isolate imaginal discs from *Him*-GAL4, UAS-BBM (UAS-palmCherry); *salm*-EGFP flies based on the green fluorescent signal. 10-12 ml of larvae in PBS were disrupted using a GentleMACS mixer (Miltenyl Biotec) and discs were collected through a mesh sieve (#0278 in, 25 opening, 710 µm). Fat was removed by centrifugation for 10 min. at 1000 rpm at 4ºC, discs were rinsed in PBS and then re-suspended in HBSS. Discs were further purified on a Ficoll gradient (25%:16%). Discs were then sorted on a Large Particle Flow Cytometer (BioSorter (FOCA1000), Union Biometrica, Inc.), obtaining 600-1000 discs per sample. Discs were spun for 5 min at 600 rcf in a Teflon Eppendorf tube and then re-suspended in the dissociation mixture (200 µl of 10x Trypsin, 200 µl HBSS, 50 µl collagenase (10 mg/mL), 50 µl dispase (10 mg/ml)). The tube was incubated for 10 min. at RT and then transferred to a thermal shaker for 30 min. at 25°C at 650 rpm. Myoblasts were filtered through a 35 µm tube-cap filter and spun at 600 rcf for 5 min. to pellet the cells. Cells were re-suspended in HBSS for evaluation or frozen in TriPure reagent for RNA extraction. We obtained samples with ~90% purity based on counting the number of red fluorescent cells / non-fluorescent + green fluorescent cells in 3 slide regions. mRNA was isolated in TriPure reagent and sequenced as described above, generating the Myo2 and Myo3 samples.

Analysis of RNA-Seq data

732 FASTA files were de-multiplexed and base called using Illumina software. Reads were
733 trimmed using the FASTX-toolkit. Sequences were mapped using STAR (Dobin et al.,
734 2013) to the *Drosophila* genome (BDGP6.80 from ENSEMBL). Mapped reads were
735 sorted and indexed using SAMtools (Li et al., 2009), and then bam files were converted
736 to bigwig files. Libraries were normalized based on library size and read-counts uploaded
737 to the UCSC Browser for visualization.

738 Mapped sequences were run through featureCounts (Liao et al., 2014) and
739 differential expression analysis was performed on the raw counts using DESeq2 (Love et
740 al., 2014). We performed all pairwise comparisons across the time-course as well as
741 between wild-type and *salmIR* samples (Supplementary Tables 1 and 4). All original and
742 processed data can be found as supplemental data or in the Gene Expression Omnibus
743 submission (accession number GSE107247). R packages employed in the analysis
744 include ComplexHeatmap (Gu et al., 2016), CorrPlot (https://github.com/taiyun/corrplot),
745 VennDiagram (Chen and Boutros, 2011), plyr (Wickham, 2011), reshape2 (Wickham,
746 2007), ggplot2 (Wickham, 2009) and RColorBrewer (Neuwirth, 2015).

747 Genome-wide soft clustering was performed in R with Mfuzz (Futschik and
748 Carlisle, 2005), using the DESeq2 normalized count values. We filtered the dataset to
749 include all genes expressed at one time point or more, defining expression as >100 counts
750 after normalization. We then set all count values <100 to 0, to remove noise below the
751 expression threshold. DESeq2 normalized data was standardized in Mfuzz to have a
752 mean value of zero and a standard deviation of one, to remove the influence of expression
753 magnitude and focus on the expression dynamics. We tested "k" ranging from 10-256.
754 We then performed consecutive rounds of clustering to obtain 3 independent replicates

with similar numbers of iterations, ultimately selecting a final k=40 clusters with iterations equal to 975, 1064 and 1118. We calculated a "stability score" for each cluster by calculating how many genes are found in the same cluster in each run (Supplementary File 1). Figures are from the 1064 iterations dataset. Mfuzz cluster core expression profiles were calculated as the average standard-normal expression of all genes with a membership value greater than or equal to 0.8, and then core profiles were clustered in R using Euclidean distance and complete linkage.

Enrichment analysis was performed with GO-Elite (Zambon et al., 2012) using available Gene Ontology terms for *Drosophila*. We additionally defined user provided gene lists for transcription factors, RNA binding proteins, microtubule associated proteins, sarcomeric proteins, genes with an RNAi phenotype in muscle (Schnorrer et al., 2010), mitochondrial genes (http://mitoXplorer.biochem.mpg.de) and *salm* core fibrillar genes (Spletter et al., 2015). Full results and gene lists are available in Supplementary File 2. These user-supplied lists allowed us to define more complete gene sets relevant to a particular process or with a specific localization than available in existing GO terms. Analysis was performed with 5000 iterations to generate reliable significance values.

Data availability

Processed data from DESeq2, Mfuzz and GO-Elite are available in Supplementary Files 1, 2, 4. mRNA-Seq data are publicly available from NCBI's Gene Expression Omnibus (GEO) under accession number GSE107247. mRNA-Seq read counts are further publicly accessible as track hubs in the UCSC Genome Browser at the following links: [1] (wild-type IFM time course)

http://genome.ucsc.edu/cgi-bin/hgTracks?hgS_doOtherUser=submit&hgS_otherUserName=Ayeroslaviz&hgS_otherUserSessionName=IFMTP.leg.TCpaperHub1 and [2] (salm timecourse) http://genome.ucsc.edu/cgi-bin/hgTracks?hgS_doOtherUser=submit&hgS_otherUserName=Ayeroslaviz&hgS_otherUserSessionName=AretSalmIFMTP.TCpaperHub2

Fiji scripts for analysis of sarcomere length, myofibril width and myofibril diameter are available from https://imagej.net/MyofibrilJ. Raw data used to generate all plots presented in figure panels are available in the source data files for Figures 1, 5, 6, 7 and 8. Data on statistical test results are presented in Supplementary File 5.

Acknowledgements

We thank Irene Ferreira for constructing the tagged *kon-tiki* allele and the Bloomington and VDRC stock centers for fly stocks. We are grateful to Reinhard Fässler and Andreas Ladurner for generous support and to Bettina Stender for excellent technical assistance. We thank Elena Nikonova for initial analysis of the *Act88F*-GAL4 x *salmIR* phenotype and Sandra Esser for testing the *salm* KK181052 hairpin. We acknowledge the VBCF (Vienna, AT) for mRNA-sequencing and the Core Facility Bioimaging at the Max Planck Institute for Biochemistry and the LMU Biomedical Center (Martinsried, DE) for help with confocal image analysis. We thank Florian Marty for help with the BioSorter, and Alexander Stark for help setting-up the mRNA-sequencing. We thank Aynur Kaya-Copur

and Wouter Koolhaas for helpful discussions, and Nuno Luis and Vincent Loreau for insightful comments on the manuscript. Our work was supported by the Max Planck Society and the CNRS; postdoctoral Humboldt, EMBO long-term (688-2011), and NIH-NRSA (5F32AR062477) fellowships (M.L.S.), the Frederich-Bauer Stiftung (M.L.S.), the Center for Integrated Protein Science München (M.L.S.); a Career Development Award from the Human Frontier Science Program (F.S.), the EMBO Young Investigator Program (F.S.) and the European Research Council under the European Union's Seventh Framework Programme (FP/2007-2013) / ERC Grant 310939 (F.S), the excellence initiative Aix-Marseille University AMIDEX (ANR-11-IDEX-0001-02) (F.S.), the ANR-ACHN (F.S.) and the LabEX-INFORM (ANR-11- LABX-0054) (F.S.) and France Bioimaging (ANR-10-INBS-04- 01) (FS).

Conflict of interest

The authors declare that they have no conflict of interest.

816 **References.**

817 Anant, S., Roy, S., and VijayRaghavan, K. (1998). Twist and Notch negatively regulate
818 adult muscle differentiation in Drosophila. Development *125*, 1361.

819 Asano, T., Ishizuka, T., Morishima, K., and Yawo, H. (2015). Optogenetic induction of
820 contractile ability in immature C2C12 myotubes. Sci Rep *5*, 8317.

821 Bate, M., Rushton, E., and Currie, D.A. (1991). Cells with persistent twist expression are
822 the embryonic precursors of adult muscles in Drosophila. Development *113*, 79–89.

823 Brinegar, A.E., Xia, Z., Loehr, J.A., Li, W., Rodney, G.G., and Cooper, T.A. (2017).
824 Extensive alternative splicing transitions during postnatal skeletal muscle development
825 are required for calcium handling functions. eLife *6*, 399.

826 Bryantsev, A.L., Baker, P.W., Lovato, T.L., Jaramillo, M.S., and Cripps, R.M. (2012).
827 Differential requirements for Myocyte Enhancer Factor-2 during adult myogenesis in
828 Drosophila. Developmental Biology *361*, 191–207.

829 Bullard, B., and Pastore, A. (2011). Regulating the contraction of insect flight muscle. J
830 Muscle Res Cell Motil *32*, 303–313.

831 Bullard, B., Burkart, C., Labeit, S., and Leonard, K. (2005). The function of elastic
832 proteins in the oscillatory contraction of insect flight muscle. J Muscle Res Cell Motil *26*,
833 479–485.

834 Burkart, C., Qiu, F., Brendel, S., Benes, V., Hååg, P., Labeit, S., Leonard, K., and
835 Bullard, B. (2007). Modular proteins from the Drosophila sallimus (sls) gene and their
836 expression in muscles with different extensibility. Journal of Molecular Biology *367*,
837 953–969.

838 Cardone, G. (2018). MyofibrilJ. GitHub. https://github.com/giocard/MyofibrilJ. 1dbb0d4.

839 Chen, H., and Boutros, P.C. (2011). VennDiagram: a package for the generation of
840 highly-customizable Venn and Euler diagrams in R. BMC Bioinformatics *12*, 35.

841 Ciciliot, S., and Schiaffino, S. (2010). Regeneration of mammalian skeletal muscle. Basic
842 mechanisms and clinical implications. Curr. Pharm. Des. *16*, 906–914.

843 Clark, I.E., Dodson, M.W., Jiang, C., Cao, J.H., Huh, J.R., Seol, J.H., Yoo, S.J., Hay,
844 B.A., and Guo, M. (2006). Drosophila pink1 is required for mitochondrial function and
845 interacts genetically with parkin. Nature *441*, 1162–1166.

846 Dietzl, G., Chen, D., Schnorrer, F., Su, K.-C., Barinova, Y., Fellner, M., Gasser, B.,
847 Kinsey, K., Oppel, S., Scheiblauer, S., et al. (2007). A genome-wide transgenic RNAi
848 library for conditional gene inactivation in Drosophila. Nature *448*, 151–156.

849 Dobin, A., Davis, C.A., Schlesinger, F., Drenkow, J., Zaleski, C., Jha, S., Batut, P.,

Chaisson, M., and Gingeras, T.R. (2013). STAR: ultrafast universal RNA-seq aligner. Bioinformatics *29*, 15–21.

Drexler, H.C.A., Ruhs, A., Konzer, A., Mendler, L., Bruckskotten, M., Looso, M., Gunther, S., Boettger, T., Kruger, M., and Braun, T. (2012). On Marathons and Sprints: An Integrated Quantitative Proteomics and Transcriptomics Analysis of Differences Between Slow and Fast Muscle Fibers. Molecular & Cellular Proteomics *11*, M111.010801–M111.010801.

Du, A., Sanger, J.M., and Sanger, J.W. (2008). Cardiac myofibrillogenesis inside intact embryonic hearts. Developmental Biology *318*, 236–246.

Dutta, D., Anant, S., Ruiz-Gómez, M., and Bate, M. (2004). Founder myoblasts and fibre number during adult myogenesis in Drosophila. Development *131*, 3761–3772.

Ehler, E., and Gautel, M. (2008). The sarcomere and sarcomerogenesis. Adv. Exp. Med. Biol. *642*, 1–14.

Fernandes, J., Bate, M., and VijayRaghavan, K. (1991). Development of the indirect flight muscles of Drosophila. Development *113*, 67–77.

Filardo, P., and Ephrussi, A. (2003). Bruno regulates gurken during Drosophila oogenesis. Mechanisms of Development *120*, 289–297.

Förster, D., and Luschnig, S. (2012). Src42A-dependent polarized cell shape changes mediate epithelial tube elongation in Drosophila. Nature Cell Biology *14*, 526–534.

Futschik, M.E., and Carlisle, B. (2005). Noise-robust soft clustering of gene expression time-course data. J Bioinform Comput Biol *3*, 965–988.

Gajewski, K.M., and Schulz, R.A. (2010). CF2 represses Actin 88F gene expression and maintains filament balance during indirect flight muscle development in Drosophila. PLoS ONE *5*, e10713.

Gautel, M., and Djinovic-Carugo, K. (2016). The sarcomeric cytoskeleton: from molecules to motion. J Exp Biol *219*, 135–145.

Gokhin, D.S., and Fowler, V.M. (2013). A two-segment model for thin filament architecture in skeletal muscle. Nature Reviews Molecular Cell Biology *14*, 113–119.

Goodman, J.W. (1968). Introduction to Fourier Optics Fourier Optics.

Gu, Z., Eils, R., and Schlesner, M. (2016). Complex heatmaps reveal patterns and correlations in multidimensional genomic data. Bioinformatics *32*, 2847–2849.

Hinits, Y., and Hughes, S.M. (2007). Mef2s are required for thick filament formation in nascent muscle fibres. Development *134*, 2511–2519.

Josephson, R. (2006). Comparative Physiology of Insect Flight Muscle. In Nature's Versatile Engine: Insect Flight Muscle Inside and Out, J. Vigoreaux, ed. (Georgetown, TX: Landes Bioscience)), pp. 35–43.

Katzemich, A., Liao, K.A., Czerniecki, S., and Schöck, F. (2013). Alp/Enigma Family Proteins Cooperate in Z-Disc Formation and Myofibril Assembly. PLoS Genetics *9*, e1003342.

Kelly, K.K., Meadows, S.M., and Cripps, R.M. (2002). Drosophila MEF2 is a direct regulator of Actin57B transcription in cardiac, skeletal, and visceral muscle lineages. Mechanisms of Development *110*, 39–50.

Kumar, L., and Futschik, M. (2007). Mfuzz: a software package for soft clustering of microarray data. Bioinformation *2*, 5–7.

Kühnlein, R.P., Frommer, G., Friedrich, M., Gonzalez-Gaitan, M., Weber, A., Wagner-Bernholz, J.F., Gehring, W.J., Jäckle, H., and Schuh, R. (1994). spalt encodes an evolutionarily conserved zinc finger protein of novel structure which provides homeotic gene function in the head and tail region of the Drosophila embryo. The EMBO Journal *13*, 168–179.

Lang, F., Aravamudhan, S., Nolte, H., Türk, C., Hölper, S., Müller, S., Günther, S., Blaauw, B., Braun, T., and Krüger, M. (2017). Dynamic changes in the mouse skeletal muscle proteome during denervation-induced atrophy. Disease Models & Mechanisms *10*, 881–896.

Lange, S., Ehler, E., and Gautel, M. (2006). From A to Z and back? Multicompartment proteins in the sarcomere. Trends in Cell Biology *16*, 11–18.

Leiss, D., Hinz, U., Gasch, A., Mertz, R., and Renkawitz-Pohl, R. (1988). Beta 3 tubulin expression characterizes the differentiating mesodermal germ layer during Drosophila embryogenesis. Development *104*, 525–531.

Lemke, S.B., and Schnorrer, F. (2017). Mechanical forces during muscle development. Mechanisms of Development *144*, 92–101.

Lemke, S.B., and Schnorrer, F. (2018). In Vivo Imaging of Muscle-tendon Morphogenesis in Drosophila Pupae. JoVE e57312–e57312.

Li, H., Handsaker, B., Wysoker, A., Fennell, T., Ruan, J., Homer, N., Marth, G., Abecasis, G., Durbin, R., 1000 Genome Project Data Processing Subgroup (2009). The Sequence Alignment/Map format and SAMtools. Bioinformatics *25*, 2078–2079.

Liao, Y., Smyth, G.K., and Shi, W. (2014). featureCounts: an efficient general purpose program for assigning sequence reads to genomic features. Bioinformatics *30*, 923–930.

Liotta, D., Han, J., Elgar, S., Garvey, C., Han, Z., and Taylor, M.V. (2007). The Him

Gene Reveals a Balance of Inputs Controlling Muscle Differentiation in Drosophila. Current Biology *17*, 1409–1413.

Llewellyn, M., Llewellyn, M.E., Barretto, R.P.J., Barretto, R., Delp, S., Delp, S.L., Schnitzer, M.J., and Schnitzer, M. (2008). Minimally invasive high-speed imaging of sarcomere contractile dynamics in mice and humans. Nature *454*, 784–788.

Loison, O., Weitkunat, M., Kaya-Copur, A., Nascimento-Alves, C., Matzat, T., Spletter, M.L., Luschnig, S., Lenne, P.-F., and Schnorrer, F. (2018). Polarization-resolved microscopy reveals a muscle myosin motor-independent mechanism of molecular actin ordering during sarcomere maturation. PLoS Biol *16*, e2004718.

Love, M.I., Huber, W., and Anders, S. (2014). Moderated estimation of fold change and dispersion for RNA-seq data with DESeq2. Genome Biology *15*, 550.

Marty, F., Rockel-Bauer, C., Simigdala, N., Brunner, E., and Basler, K. (2014). Large-scale imaginal disc sorting: A protocol for "omics-"approaches. Methods *68*, 260–264.

Mas, J.A., Vivar, J., Arredondo, J.J., and Cervera, M. (2008). CF2 activity and enhancer integration are required for proper muscle gene expression in Drosophila. Mechanisms of Development *125*, 617–630.

Mazelet, L., Parker, M.O., Li, M., Arner, A., and Ashworth, R. (2016). Role of Active Contraction and Tropomodulins in Regulating Actin Filament Length and Sarcomere Structure in Developing Zebrafish Skeletal Muscle. Front Physiol *7*, 91.

Montfort, J., Le Cam, A., Gabillard, J.-C., and Rescan, P.-Y. (2016). Gene expression profiling of trout regenerating muscle reveals common transcriptional signatures with hyperplastic growth zones of the post-embryonic myotome. BMC Genomics *17*, 810.

Neuwirth, E. (2015). Package "RColorBrewer." 1–5.

Ni, J.-Q., Zhou, R., Czech, B., Liu, L.-P., Holderbaum, L., Yang-Zhou, D., Shim, H.-S., Tao, R., Handler, D., Karpowicz, P., et al. (2011). A genome-scale shRNA resource for transgenic RNAi in Drosophila. Nature Methods *8*, 405–407.

Orfanos, Z., and Sparrow, J.C. (2013). Myosin isoform switching during assembly of the Drosophila flight muscle thick filament lattice. Journal of Cell Science *126*, 139–148.

Orfanos, Z., Leonard, K., Elliott, C., Katzemich, A., Bullard, B., and Sparrow, J. (2015). Sallimus and the Dynamics of Sarcomere Assembly in Drosophila Flight Muscles. Journal of Molecular Biology *427*, 2151–2158.

Pérez-Moreno, J.J., Bischoff, M., Martín-Bermudo, M.D., and Estrada, B. (2014). The conserved transmembrane proteoglycan Perdido/Kon-tiki is essential for myofibrillogenesis and sarcomeric structure in Drosophila. Journal of Cell Science *127*, 3162–3173.

953 Potthoff, M.J., Arnold, M.A., McAnally, J., Richardson, J.A., Bassel-Duby, R., and
954 Olson, E.N. (2007). Regulation of skeletal muscle sarcomere integrity and postnatal
955 muscle function by Mef2c. Molecular and Cellular Biology *27*, 8143–8151.

956 Racca, A.W., Klaiman, J.M., Pioner, J.M., Cheng, Y., Beck, A.E., Moussavi-Harami, F.,
957 Bamshad, M.J., and Regnier, M. (2016). Contractile properties of developing human fetal
958 cardiac muscle. J. Physiol. (Lond.) *594*, 437–452.

959 Reedy, M.C., and Beall, C. (1993). Ultrastructure of developing flight muscle in
960 Drosophila. I. Assembly of myofibrils. Developmental Biology *160*, 443–465.

961 Reedy, M., Bullard, B., and Vigoreaux, J. (2000). Flightin is essential for thick filament
962 assembly and sarcomere stability in Drosophila flight muscles. Journal of Cell Biology
963 *151*, 1483.

964 Regev, G.J., Kim, C.W., Tomiya, A., Lee, Y.P., Ghofrani, H., Garfin, S.R., Lieber, R.L.,
965 and Ward, S.R. (2011). Psoas Muscle Architectural Design, In Vivo Sarcomere Length
966 Range, and Passive Tensile Properties Support Its Role as a Lumbar Spine Stabilizer.
967 Spine *36*, E1666–E1674.

968 Roper, K., Mao, Y., and Brown, N. (2005). Contribution of sequence variation in
969 Drosophila actins to their incorporation into actin-based structures in vivo. Journal of
970 Cell Science *118*, 3937.

971 Sandmann, T., Jensen, L., Jakobsen, J., Karzynski, M., Eichenlaub, M., Bork, P., and
972 Furlong, E. (2006). A temporal map of transcription factor activity: mef2 directly
973 regulates target genes at all stages of muscle development. Developmental Cell *10*, 797–
974 807.

975 Sanger, J.W., Wang, J., Fan, Y., White, J., Mi-Mi, L., Dube, D.K., Sanger, J.M., and
976 Pruyne, D. (2017). Assembly and Maintenance of Myofibrils in Striated Muscle. Handb
977 Exp Pharmacol *235*, 39–75.

978 Sanger, J.W., Wang, J., Holloway, B., Du, A., and Sanger, J.M. (2009).
979 Myofibrillogenesis in skeletal muscle cells in zebrafish. Cell Motil. Cytoskeleton *66*,
980 556–566.

981 Sarov, M., Barz, C., Jambor, H., Hein, M.Y., Schmied, C., Suchold, D., Stender, B.,
982 Janosch, S., K J, V.V., Krishnan, R.T., et al. (2016). A genome-wide resource for the
983 analysis of protein localisation in Drosophila. eLife *5*, e12068.

984 Schiaffino, S., and Reggiani, C. (2011). Fiber Types in Mammalian Skeletal Muscles.
985 Physiological Reviews *91*, 1447–1531.

986 Schiaffino, S., Rossi, A.C., Smerdu, V., Leinwand, L.A., and Reggiani, C. (2015).
987 Developmental myosins: expression patterns and functional significance. Skeletal Muscle
988 1–14.

989 Schindelin, J., Arganda-Carreras, I., Frise, E., Kaynig, V., Longair, M., Pietzsch, T.,
990 Preibisch, S., Rueden, C., Saalfeld, S., Schmid, B., et al. (2012). Fiji: an open-source
991 platform for biological-image analysis. Nature Methods *9*, 676–682.

992 Schnorrer, F., Kalchhauser, I., and Dickson, B. (2007). The transmembrane protein Kon-
993 tiki couples to Dgrip to mediate myotube targeting in Drosophila. Developmental Cell *12*,
994 751–766.

995 Schnorrer, F., Schönbauer, C., Langer, C.C.H., Dietzl, G., Novatchkova, M.,
996 Schernhuber, K., Fellner, M., Azaryan, A., Radolf, M., Stark, A., et al. (2010).
997 Systematic genetic analysis of muscle morphogenesis and function in Drosophila. Nature
998 *464*, 287–291.

999 Schönbauer, C., Distler, J., Jährling, N., Radolf, M., Dodt, H.-U., Frasch, M., and
1000 Schnorrer, F. (2011). Spalt mediates an evolutionarily conserved switch to fibrillar
1001 muscle fate in insects. Nature *479*, 406–409.

1002 Sevdali, M., Kumar, V., Peckham, M., and Sparrow, J. (2013). Human congenital
1003 myopathy actin mutants cause myopathy and alter Z-disc structure in Drosophila flight
1004 muscle. Neuromuscular Disorders *23*, 243–255.

1005 Shwartz, A., Dhanyasi, N., Schejter, E.D., and Shilo, B.-Z. (2016). The Drosophila
1006 formin Fhos is a primary mediator of sarcomeric thin-filament array assembly. eLife *5*,
1007 D786.

1008 Soler, C., and Taylor, M. (2009). The Him gene inhibits the development of Drosophila
1009 flight muscles during metamorphosis. Mechanisms of Development *126*, 595–603.

1010 Soler, C., Han, J., and Taylor, M.V. (2012). The conserved transcription factor Mef2 has
1011 multiple roles in adult Drosophila musculature formation. Development *139*, 1270–1275.

1012 Sparrow, J., and Schöck, F. (2009). The initial steps of myofibril assembly: integrins
1013 pave the way. Nature Reviews Molecular Cell Biology *10*, 293–298.

1014 Spletter, M.L., and Schnorrer, F. (2014). Transcriptional regulation and alternative
1015 splicing cooperate in muscle fiber-type specification in flies and mammals. Experimental
1016 Cell Research *321*, 90–98.

1017 Spletter, M.L., Barz, C., Yeroslaviz, A., Schönbauer, C., Ferreira, I.R.S., Sarov, M.,
1018 Gerlach, D., Stark, A., Habermann, B.H., and Schnorrer, F. (2015). The RNA-binding
1019 protein Arrest (Bruno) regulates alternative splicing to enable myofibril maturation in
1020 Drosophila flight muscle. EMBO Rep *16*, 178–191.

1021 Stronach, B.E., Renfranz, P.J., Lilly, B., and Beckerle, M.C. (1999). Muscle LIM
1022 proteins are associated with muscle sarcomeres and require dMEF2 for their expression
1023 during Drosophila myogenesis. Molecular Biology of the Cell *10*, 2329–2342.

1024 Syme, D., and Josephson, R. (2002). How to build fast muscles: synchronous and

1025 asynchronous designs. Integrative and Comparative Biology *42*, 762.

1026 Tanaka, K.K.K., Bryantsev, A.L., and Cripps, R.M. (2008). Myocyte enhancer factor 2
1027 and chorion factor 2 collaborate in activation of the myogenic program in Drosophila.
1028 Molecular and Cellular Biology *28*, 1616–1629.

1029 Toydemir, R.M., Rutherford, A., Whitby, F.G., Jorde, L.B., Carey, J.C., and Bamshad,
1030 M.J. (2006). Mutations in embryonic myosin heavy chain (MYH3) cause Freeman-
1031 Sheldon syndrome and Sheldon-Hall syndrome. Nat Genet *38*, 561–565.

1032 Tskhovrebova, L., and Trinick, J. (2003). Titin: properties and family relationships.
1033 Nature Reviews Molecular Cell Biology *4*, 679–689.

1034 Vigoreaux, J.O. (2006). Molecular Basis of Muscle Structure. In Muscle Development in
1035 Drosophila, (New York, NY: Springer New York), pp. 143–156.

1036 Wallgren-Pettersson, C., Sewry, C.A., Nowak, K.J., and Laing, N.G. (2011). Nemaline
1037 myopathies. Semin Pediatr Neurol *18*, 230–238.

1038 Warren, G.L., Summan, M., Gao, X., Chapman, R., Hulderman, T., and Simeonova, P.P.
1039 (2007). Mechanisms of skeletal muscle injury and repair revealed by gene expression
1040 studies in mouse models. J. Physiol. (Lond.) *582*, 825–841.

1041 Weitkunat, M., and Schnorrer, F. (2014). A guide to study Drosophila muscle biology.
1042 Methods *68*, 2–14.

1043 Weitkunat, M., Brasse, M., Bausch, A.R., and Schnorrer, F. (2017). Mechanical tension
1044 and spontaneous muscle twitching precede the formation of cross-striated muscle in vivo.
1045 Development *144*, 1261–1272.

1046 Weitkunat, M., Kaya-Copur, A., Grill, S.W., and Schnorrer, F. (2014). Tension and
1047 force-resistant attachment are essential for myofibrillogenesis in Drosophila flight
1048 muscle. Curr Biol *24*, 705–716.

1049 Wickham, H. (2009). ggplot2: Elegant Graphics for Data Analysis (Springer).

1050 Wickham, H. (2007). Reshaping Data with the reshapePackage. Journal of Statistical
1051 Software *21*, 1–20.

1052 Wickham, H. (2011). The Split-Apply-Combine Strategy for Data Analysis. Journal of
1053 Statistical Software *40*, 1–29.

1054 Yang, J. (2018). SALL4 as a transcriptional and epigenetic regulator in normal and
1055 leukemic hematopoiesis. Biomark Res *6*, 1.

1056 Zambon, A.C., Gaj, S., Ho, I., Hanspers, K., Vranizan, K., Evelo, C.T., Conklin, B.R.,
1057 Pico, A.R., and Salomonis, N. (2012). GO-Elite: a flexible solution for pathway and
1058 ontology over-representation. Bioinformatics *28*, 2209–2210.

1059 Zappia, M.P., and Frolov, M.V. (2016). E2F function in muscle growth is necessary and
1060 sufficient for viability in Drosophila. Nature Communications *7*, 10509.

1061 Zhang, X., Yuan, X., Zhu, W., Qian, H., and Xu, W. (2015). SALL4: An emerging
1062 cancer biomarker and target. Cancer Letters *357*, 55–62.

1063 Zhao, Y., Li, J., Liu, H., Xi, Y., Xue, M., Liu, W., Zhuang, Z., and Lei, M. (2015).
1064 Dynamic transcriptome profiles of skeletal muscle tissue across 11 developmental stages
1065 for both Tongcheng and Yorkshire pigs. BMC Genomics *16*, 377.

1066 Zheng, Q., Zhang, Y., Chen, Y., Yang, N., Wang, X.-J., and Zhu, D. (2009). Systematic
1067 identification of genes involved in divergent skeletal muscle growth rates of broiler and
1068 layer chickens. BMC Genomics *10*, 87.

1069

Figure Legends

Figure 1. Development of the dorsal longitudinal indirect flight muscles

(A-H) Time-course of DLM development. (A) Myoblasts adhering to the hinge of the larval wing disc were visualised with *Him*-Gma-GFP (green), F-actin was stained with phalloidin (red) and nuclei with DAPI (blue). (B-H) Time-course of DLM and myotendinous junction development at 16h (B), 24h (C), 32h (D), 48h (E), 56h (F), 72h (G) and 90h APF (H). F-actin was stained with phalloidin (red), Shot (green) and βPS-Integrin (blue). DLMs are highlighted in dashed yellow lines in B an C. (A'''-C''') Scheme of the respective developmental stages with myoblasts and muscles in red, tendon cells in blue and wing disc or pupal thorax outline in black. The length of the muscle fibers in indicated in red. For details see text. Scale bar represents 100 μm. (**I**) Temporal summary of known events during myogenesis (red). Samples for mRNA-Seq were collected at time points noted in black.

Figure 2. Verification of mRNA-Seq time-course by 'indicator' gene expression

(A,D,G,J,M,P,S) Temporal expression dynamics were evaluated by clustering standard-normal mRNA-seq counts using Mfuzz. Temporal expression profiles are plotted with high membership values in warm colours (red, pink), and lower membership values in cool colours (blue, green). **(B,E,H,K,N,Q,T)** The profile of one 'indicator' gene from each cluster is shown and coloured based on the Mfuzz membership value α. **(C,F,I,L,O,R,U).** Protein expression and localisation dynamics were visualised by antibody staining against Twi (C) and Aret (F) or against GFP for GFP tagged fosmid reporters for Kon (I), β-Tub60D (L), βPS-Integrin (*mys*) (O), Unc-89 (Obscurin) (R) and

Strn-Mlck (U). Images for the same protein were acquired using the same settings, and pseudo-coloured based on intensity. Note the close correlation between mRNA and protein expression dynamics. Time points are indicated by blue dots on the mRNA expression profile. Scale bars represent 20 μm.

Figure 2 – Supplement 1. Forty distinct temporal mRNA-Seq expression profiles

Temporal expression profiles were identified by clustering standard-normal mRNA-Seq counts using Mfuzz to group genes with similar temporal expression dynamics. Expression dynamic profiles were labelled 1-40. Each plot shows the profile for each gene in the cluster, with profiles of genes with high membership values in warm colours (red, pink) and lower membership values in cool colours (blue, green).

Figure 2 – Supplement 2. Additional examples of 'indicator' gene expression

(A-P) Cluster profiles and mRNA dynamics for additional indicator genes. *salm* from cluster 26 (A,B), *rhea* (Talin) from cluster 25 (D,E), *fln* from cluster 3 (G,H) and *Mhc*, *Act88F*, *Mf* from cluster 22 (J,K,M,O) are shown. The respective protein dynamics were visualised with antibodies against the respective protein or GFP fusion protein (C,F,I,L,N,P). Note that although Mhc and Act88F show significant mRNA and protein expression already at 30 h APF, this expression dramatically increases after 30 h APF to reach even higher protein levels at 72 h APF. Fln and Mf mRNA and protein are only induced to high levels after 30 h APF. Scale bars represent 20 μm.

Figure 3. Expression dynamics reveal a temporal ordering of biological processes during muscle morphogenesis

(**Top**) Heat map of Mfuzz cluster core expression profiles. Standard-normal count values for all genes with a membership value $\alpha > 0.8$ were averaged to generate the core expression profile for each cluster. Mfuzz expression profiles fall into 8 groups (coloured dendrogram leaves) based on hierarchical clustering of their temporal expression dynamics. Time points and Mfuzz clusters are labelled. Colour scale of standard-normal count values ranges from blue (stable/no expression) to red (high expression). (**Bottom**) GO Biological Process and user-defined gene set (marked with *) enrichments calculated with GO-Elite. Note that proliferation, development and differentiation terms are enriched at early time points, while mitochondrial and sarcomere terms are enriched at late time points. A coloured box indicates a significant enrichment of a given term in the specified cluster (see Supplementary File 2 for details).

Figure 4. A major transition in gene expression after 30 h APF

(**A**) DESeq2 principle components analysis (PCA) of all mRNA-Seq libraries. Each triangle represents a different biological replicate coloured by time point. Note that individual replicates for a given time point cluster together. PC1 divides early (≤48 h APF) from late (≥72 h) stages. (**B**) Stacked box plot of the number of significantly differentially expressed genes up-regulated (reds) or down-regulated (blues) between sequential time points with a p-value <0.05 and a $\log_2$FC (fold change) of >1 (dark), >2 (medium) or >5 (light). The large differences between myoblast to 16 h APF reflect muscle specification. A second large shift in expression is evident between 30 h and 72 h

APF. (**C**) Volcano plot illustrating the strong up-regulation of sarcomeric proteins (red) from 30 h to 72 h APF. Significantly up- or down-regulated genes are in blue (p-value <0.05 and abs(log_2FC) >2). (**D**) Hierarchical clustering of log_2 transformed DESeq2 normalized counts for all genes that are significantly up-regulated between 30 h and 72 h APF. Note that they are either strongly induced at 48 h or 72 h APF (from yellow to red), or only turned on at 48 h or 72 h APF (blue to yellow/red), suggesting a major transition in gene expression after 30 h APF. Colour scale of log_2 count values ranges from blue (not expressed) to red (highly expressed). (**E**) GO-Elite and user-defined gene set (marked with *) enrichments in up- (red) and down- (blue) regulated genes from 30 h to 72 h APF. Note the strong enrichment of mitochondrial and sarcomere terms in the up-regulated genes. (**F**) Pie charts showing the proportion of genes belonging to an enriched Mfuzz cluster in the sets of genes either up- or down-regulated from 30 h - 72 h APF. Note that a large proportion of genes up-regulated 30 h - 72 h belong to cluster 22, as well as Mfuzz clusters enriched for sarcomere (yellow) or mitochondrial (green) terms.

Figure 4 – Supplement 1. Additional evidence supporting a transition in gene expression between 30 h and 72 h APF

(**A**) Principle component analysis (PCA) of Mfuzz clusters. PC1 largely separates clusters based on 30 h to 72 h dynamics, with significantly "up-regulated" clusters on the left (red) and "down regulated" clusters on the right (green) (see Figure 4F). Sarcomeric and mitochondrial gene clusters shown in yellow script. (**B**) Number of differentially expressed (DE) genes that are the same between time points. Total number of DE genes on bottom. Note that sequential time points share the greatest overlap. (**C,D**) Venn

diagrams showing the strong overlap between genes coding for sarcomeric proteins, *salm* core genes, Mfuzz cluster 22 and genes up-regulated (C) but not down-regulated (D) between 30 h and 72 h APF.

Figure 5. Sequential phases of sarcomere morphogenesis in flight muscles

(**A**) Scheme of hemi-thoraces at 34 h, 48 h, 60 h, 72 h, 80 h, 90 h APF and 1 day adults (muscle in red, tendon in blue, sarcomeres in yellow) with indicated muscle fiber length. Myofibrils and sarcomeres at these time points were stained for phalloidin (F-actin, red) and Kettin (Z-disc, green). Scale bar represents 5 µm. (**B,C**) Tukey box and whisker plot of sarcomere length and myofibril width. Box extends from 25% to 75%, line marks median, whiskers extend to 25/75% plus 1.5 times the interquartile range. (**D**) Histogram of sarcomere number per myofibril. Error bars represent SD. Note the sarcomere assembly at 34 h, followed by sarcomere addition until ~48 h and sarcomere maturation after ~48 h APF. (**E**) Cross-sections of the DLMs at 30 h, 48 h, 60 h, 72 h, 80 h, 90 h APF and 1 day adult. Scale bar represents 5 µm. (**F,G**) Tukey box and whisker plot of myofibril diameter and myofiber cross-sectional area. Note the lack of growth in diameter or area from 30 h to 48 h. (**H**) Histogram of the number of myofibrils per myofiber. Error bars represent SD. Note that all myofibrils are already present at 30 h APF. Tukey's multiple comparison p-value <.05*, .01**, .001***, n.s. = not significant. N>10 for each individual time point. (**I**) Stills of live movies of DLMs at 30 h, 36 h, 42 h, 48 h, 60 h and 72 h APF. Scale bar represents 50 µm. For live movies see Movie 1. Stills are a time 0.0 s image (magenta) overlaid with a time +0.65 s image (green), where a perfect overlap (white) shows no movement. (**J**) Quantification of spontaneous

contraction events per fiber per 5 minutes, with single twitches in blue and double twitches in green. Fibers are first contractile at 30 h APF, reach peak contractility at 48 h and stop all spontaneous contraction shortly after 60 h APF.

Figure 5 – Supplement 1. Expression and localisation of thin- and thick-filament structural proteins

(**A-E**) Developing flight muscle myofibrils are stained with phalloidin (red) and the respective sarcomeric proteins (green). Flightin (A) cannot be detected at 30 h, but decorates the thick filament from 48 h APF. Unc-89/Obscurin-GFP (B) labels the M-line from 30 h, and is markedly refined to 72 h APF. Myosin heavy chain (C) is visible in a regular pattern at 30 h APF. Myofilin/Mf (D) cannot be detected at 30 h and decorates the thick filament at 48 h APF. Likewise, IFM-specific Strn-Mlck Isoform R (E) is not expressed at 30 h, but is detected on the thick filament at low levels at 48 h APF. Scale bars represent 5 μm.

Figure 5 - Movie 1. Twitching time-course in developing DLMs

Confocal movies of spontaneous contraction (twitching) in developing DLMs at 30 h, 36 h, 42 h, 48 h, 60 h and 72 h APF. Fibers are the same as those shown in Figure 5I. Muscle attachments are visualized using a Talin-YPet fusion, which is enriched at the muscle end. Note that fibers weakly contract at 30 h and increase in contraction intensity and frequency until 48 h APF, but then completely stop all contraction by 72 h APF. Scale bar represents 20 μm. Individual movie duration (in seconds) as noted.

Figure 6. *salm* contributes to the transition in gene expression after 30 h APF.

(**A**) Volcano plot of mRNA-Seq comparison of wild-type (WT) versus *salmIR* IFMs at 72 h APF. Note the significant down-regulation of genes in *salmIR*, especially sarcomeric protein coding genes (red). Significantly differentially expressed (DE) genes (abs(log_2 FC)>2, p< 0.05) are in blue. (**B**) Violin plot showing down-regulation of sarcomeric proteins (in red), mitochondrial proteins (in green) and members of Mfuzz cluster 22 (in yellow) in *salmIR* compared to wild type at 72 h APF. Box plots indicate the median of the data as well as the 1st and 3rd quartile in the box, outliers are the dots. (**C**) WT mRNA-Seq fold change values of all genes significantly DE from 30 h to 72 h APF are ordered from lowest to highest (black). The corresponding *salmIR* fold change is shown in yellow. Both sarcomeric (red) and mitochondrial protein coding genes (blue) are less strongly up- or down-regulated in *salmIR* across the 30 h to 72 h APF transition. Note that many genes in *salmIR* (yellow dots) are not as strongly induced or even repressed compared to WT (below and above the black WT line, respectively). (**D**) Violin plot comparing the log_2FC over the 30 h to 72 h transition in WT (in black) and *salmIR* IFM (in magenta) for members of Mfuzz Cluster22. Box plots indicate the median of the data as well as the 1st and 3rd quartile in the box, outliers are the dots. Note the significant decrease in induction to 72 h APF in the *salmIR* sample. ***Student's t-test p-value < .0005. (**E-H**) *salm* is required for the induction of some but not all sarcomeric proteins. *Act88F>>salmIR* in the background of GFP-tagged Strn-Mlck-IsoR (E), Fln (F), Mhc (G) and Unc-89 (H). Quantitative changes in live GFP fluorescence at 90 h APF were measured by quantitative confocal microscopy relative to standard fluorescent beads, revealing significant decreases in induction for Strn-Mlck, Fln and Mhc between wild

type control (shown in yellow, *Act88F*-GAL4 crossed to w^{1118}) and *Act88F>>salmIR* (shown in purple). Scale bar represents 5 µm. Error bars represent SEM, Student's t-test p-value <0.05*, 0.001***, n.s. = not significant. N>10 for each individual sample. (E'-H'') Intensity-coded GFP fluorescence at 90 h APF in confocal images of fixed myofibrils.

Figure 6 – Supplement 1. *salm* regulates gene expression during flight muscle development

(**A-C**) Volcano plots of mRNA-Seq data comparing wild-type (WT) versus *salmIR* IFMs at 24h (A), 30h (B) and 1d adult. Significantly differentially expressed (DE) genes (abs(log_2FC)>2, $p < 0.05$) are in blue. Note the significant down regulation of genes at all time points, particularly sarcomeric protein coding genes (red). (**D**) Violin plot showing down-regulation of sarcomeric proteins (in red), mitochondrial proteins (in green) and members of Mfuzz cluster 22 (in yellow) in *salmIR* compared to wild type at 30 h APF. Box plots indicate the median of the data as well as the 1st and 3rd quartile in the box, outliers are the dots. Note that all three gene groups are down-regulated in in *salmIR*. (**E**) Mfuzz cluster enrichment in genes that are DE between WT and *salmIR*. Note that the sarcomeric and mitochondrial clusters (indicated by the green and yellow dots, respectively) are all down-regulated in *salmIR*. Colour scale represents enrichment Z-score. (**F**) GO and gene set (marked with *) enrichment in genes that are DE between WT and *salmIR*. Note that terms down-regulated in *salmIR* are enriched in genes up-regulated in WT from 30 h to 72 h. (**G**) Venn diagram showing the strong overlap between

sarcomeric protein coding genes, *salm* core genes, Mfuzz cluster 22 and genes down-regulated in *salmIR* at 72 h APF.

Figure 6 – Supplement 2. *Act88F*-GAL4 driven knock-down of *salm* is efficient.

(**A-D**) At 24 h APF, both Aret and Salm expression is observed in the nuclei of wild type (A) and *Act88F>>salmIR* (B) DLMs. At 72 h APF, Salm protein is present in wild type (C) but cannot be detected in the nuclei of *Act88F>>salmIR* (D) DLMs. Scale bars represent 10 μm.

Figure 6 – Supplement 3. Expression of sarcomere proteins strongly increases from 30 h to 72 h APF.

(A-E) Live assay to quantify GFP fusion protein expression by normalizing GFP expression intensity in muscle to fluorescent beads (relative fluorescence on Y-axis). Gma-GFP expression driven by *Mef2*-GAL4 (A) shows a decrease in expression with developmental time, likely due to a decrease in expression from the Mef2 enhancer. Mhc-GFP (B) and Unc-89-GFP (C) show detectable GFP expression at 30 h APF, but a massive increase in expression to 72 h APF. Fln-GFP (D) is not detectable at 30 h APF and increases expression from 48 h APF to 72 h APF. Strn-Mlck-GFP (E) is weakly detectable at 48 h APF and is massively induced to 72 h APF. Relative fluorescence was calculated as muscle intensity/bead intensity. Error bars represent SEM, Tukey's multiple comparison p-value <0.05*, 0.001***, n.s. = not significant. N>10 flies for each timepoint.

Figure 7. *salm* is required for normal sarcomere maturation and function

(**A-H**) Myofibrils of *Act88F*-GAL4 / + (A-D) or *Act88F>>salmIR* (E-H). Note that *salmIR* DLM remains fibrillar and appears normal at 48 h APF (E), but at 72 h APF (F) 90h APF (G) and 2 day adult (H) Z-discs widen and show actin accumulations (arrowheads). (**I,J**) Tukey box and whisker plot of myofibril width (I) and sarcomere length (J) in *Act88F*-GAL4 / + and *Act88F>>salmIR* (red). Tukey's multiple comparison p-value <.001***. N>10 for each individual time point. Scale bars represent 5 μm. (**K-O**) Stills from live movies of developing DLMs at 48 h and 72 h APF in *Act88F*-GAL4 / + (K, M) and *Act88F>>salmIR* (L, N). Scale bar represents 50 μm. Coloured as in Figure 5. (O) Quantification of spontaneous contraction events per fiber per 5 minutes, with single twitches in blue and double twitches in green. Error bars represent SEM. *salmIR* fibers continue spontaneously contracting at 72 h APF.

Figure 7 - Movie 2. Twitching in developing *Act88F*-GAL4 / + and *Act88F>>salmIR* DLMs at 48h APF

Confocal movies of spontaneous contraction in *Act88F*-GAL4 / + (control) and *Act88F>>salmIR* DLMs at 48h APF. Muscle attachments are visualized using a Talin-YPet fusion. *salmIR* fibers show only a single twitch at 48 h APF, while both single and double twitches are observed in the control. Scale bar represents 20 μm.

Figure 7 – Movie 3. Twitching in developing *Act88F*-GAL4 / + and *Act88F>>salmIR* DLMs at 72h APF

72 h APF muscle ends are labelled with a Talin-YPet fusion in *Act88F*-GAL4 / + (control) and *Act88F*-GAL4 / *salmIR* DLMs. Control fibers show no contractions at 72 h APF, but *salmIR* fibers continue to contract. Scale bar represents 20 μm.

Figure 7 – Supplement 1. *Act88F>>salmIR* and *Strn-Mlck* mutant flies are flightless and IFM fibers rupture in adult flies

(A) Adult males from *Act88F*-GAL4 crossed to two independent *salmIR* hairpins as well as $Strn^{M102893}$ are flightless. **(B-J)** At 90 h APF, *Act88F*-GAL4 / + (B-D), *Act88F>>salmIR* (E-G) and $Strn^{M102893}$ (H-J) all have 6 intact fibers. At 1 day and 2 days after eclosion, both *Act88F>>salmIR* (F,G) and $Strn^{M102893}$ (I,J) show muscle tearing and atrophy. Scale bar represents 200 μm.

Figure 8. Strn-Mlck contributes to sarcomere length regulation during sarcomere maturation.

(**A-J**) Wild type (A-E) and $Strn^{M102893}$ mutant (F-J) sarcomere development at 48 h, 72 h, 80 h, 90 h APF and 1 day adult. (**K-N**) Tukey box and whisker plot of myofibril width (K) and sarcomere length (L) in wild type and $Strn^{M102893}$ mutant (red). Tukey's multiple comparison p-value <.001***. N>10 for each individual time point. Histogram of fiber length (M) and number of sarcomeres per myofibril (N). Error bars represent SEM. Tukey's multiple comparison p-value <.01**, N>10 for each individual time point. Note that a normal number of sarcomeres are formed in $Strn^{M102893}$ mutants, but they grow too long at 80 h APF and hyper-contract in 1day adult.

Figure 9. Model for ordered sarcomere morphogenesis

Phase 1 - Sarcomere assembly: Sarcomeric proteins are expressed at low levels, enabling the self-assembly of immature sarcomeres and myofibrils at around 30 h APF. Each of the 2000 myofibrils contains about 80 immature sarcomeres. **Phase 2 - Sarcomere addition**: Sarcomere protein expression increases and each immature myofibril incorporates many new sarcomeres until about 48 h APF. These immature sarcomeres contract spontaneously. **Phase 3 - Sarcomere maturation**: After 48 h APF, sarcomere protein expression increases even more, including flight muscle specific proteins/isoforms, and all sarcomeres strongly grow in width and length. This enables the flight muscle to gain stretch-activation. Muscles are shown in red, tendons in blue. Structural proteins are illustrated as cartoons and are not drawn to scale. Induction of Actin, Mhc, Myofilin, Flightin, Strn-Mlck and Unc-89/Obscurin is shown here, expression of αActinin, Projectin and Kettin/Sallimus was shown by others (Bullard et al., 2005; Burkart et al., 2007; Katzemich et al., 2013; Orfanos et al., 2015; Weitkunat et al., 2014).

Supplementary File 1. mRNA-Seq raw data

The file includes multiple tabs containing the raw or input counts data from bioinformatics analysis, as well as a key to all original data provided in the supplementary tables. This table includes mRNA-Seq counts data, DESeq2 normalized counts data and standard normal counts data used for Mfuzz clustering for wild-type and *salmIR* IFM time points. The averaged core expression profiles for each Mfuzz cluster are also listed.

Supplementary File 2. GO-Elite analysis data.

This table includes multiple tabs containing the GO-Elite analysis of enrichments in Mfuzz clusters as well as genes up- or down-regulated from 30 h - 72 h APF and between wild-type and *salmIR* IFM. It also contains a complete list of all genes included in the 'User Defined' gene sets.

Supplementary File 3. Summary of sarcomere and myofibril quantifications

This table includes a numerical summary of quantification values reported graphically in Figures 5, 7 and 8. Quantifications of sarcomere length, myofibril width and myofibril diameter were performed with the MyofibrilJ script (see Materials and Methods). Fiber length and cross-sectional area measurements were performed in Fiji/Image J.

Supplementary File 4. DESeq2 pairwise differential expression analysis

This table contains multiple tabs containing the output data from DESeq2 differential expression analysis between sequential IFM development time points, from 30-72h APF as well as between WT and *salmIR* IFM.

Supplementary File 5. Statistical Data

This table includes multiple tabs containing the statistical and calculation data for the different panels of Figures 1, 5, 6, 7 and 8.

Figure 1-source data 1

This table includes the length measurements of the indirect flight muscle fibers at the indicated stage.

Figure 5-source data 1

This table includes calculation of the number of sarcomeres per myofibril in wild type flight muscles at the indicated stage.

Figure 5-source data 2

This table includes the sarcomere length in wild type flight muscles measured at the indicated stage. Note that image analysis is limited by pixel size and thus can result in the same number.

Figure 5-source data 3

This table includes the sarcomere/myofibril width in wild type flight muscles measured at the indicated stage. Note that image analysis is limited by pixel size and thus can result in the same number.

Figure 5-source data 4

This table includes the myofiber cross-sectional area measured in wild type flight muscle fibers or only fibers 3&4 at the indicated stage.

Figure 5-source data 5

This table includes the number of myofibrils per myofiber calculated for either all wild type flight muscle fibers or only fibers 3&4 at the indicated stage.

Figure 5-source data 6

This table includes the myofibril diameter measured in wild type flight muscles at the indicated stage.

Figure 5-source data 7

This table includes the muscle twitch events per wild-type fiber per 5 minutes recorded at the indicated stage.

Figure 6-source data 1

This table includes the fiber divided by bead fluorescence intensity measurements for quantification of the indicated fosmid-GFP or UAS-Gma-GFP expression levels at the indicated stage.

Figure 6-source data 2

This table includes the fiber divided by bead fluorescence intensity measurements for various fosmid-GFPs in the *Act88F>>salmIR* or control *Act88F-Gal4 x w-* background at 90 h APF.

Figure 7-source data 1

This table includes the muscle twitch events per *Act88F>>salmIR* fiber per 5 minutes and the respective controls recorded at the indicated stage.

Figure 7-source data 2

This table includes the sarcomere length measured in *Act88F>>salmIR* flight muscles and the respective controls at the indicated stage. Note that image analysis is limited by pixel size and thus can result in the same number.

Figure 7-source data 3

This tables includes the sarcomere/myofibril width measured in *Act88F>>salmIR* flight muscles and the respective controls at the indicated stage. Note that image analysis is limited by pixel size and thus can result in the same number.

Figure 8-source data 1

This table includes the numbers of sarcomeres calculated per *strn-mlck* mutant myofibril and the respective control at the indicated stage.

Figure 8-source data 2

This table includes the length measurements of the indirect flight muscle fibers at the indicated stage for *strn-mlck* mutants and wild-type controls.

Figure 8-source data 3

This table includes the calculated numbers of sarcomeres per myofibril at the indicated stage for *strn-mlck* mutants. Note that image analysis is limited by pixel size and thus can result in the same number.

Figure 8-source data 2

This table includes the sarcomere length measured in *strn-mlck* mutant flight muscles at the indicated stage. Note that image analysis is limited by pixel size and thus can result in the same number.

Spletter *et al.*, Figure 1

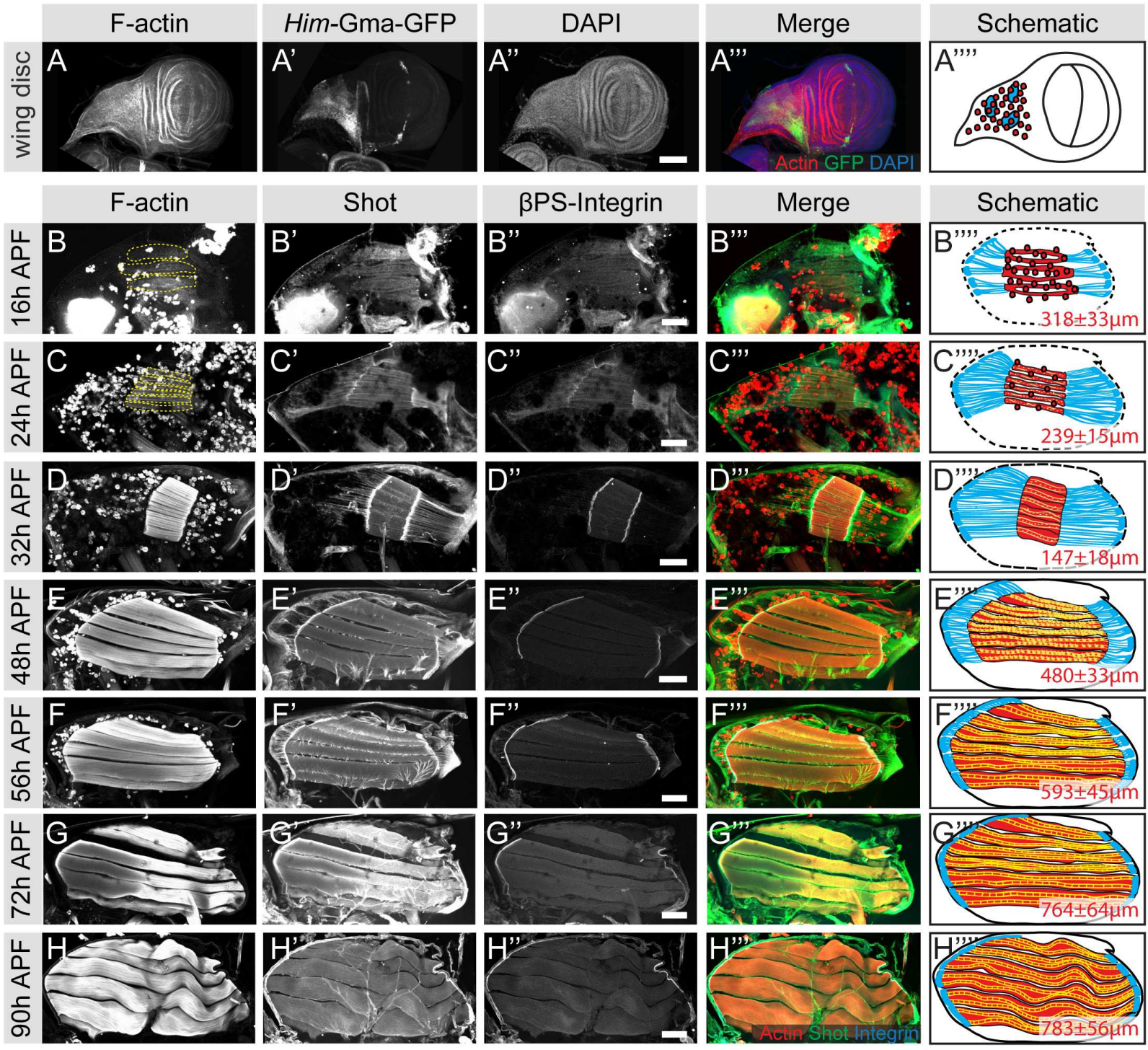

I Time-course of indirect flight muscle development

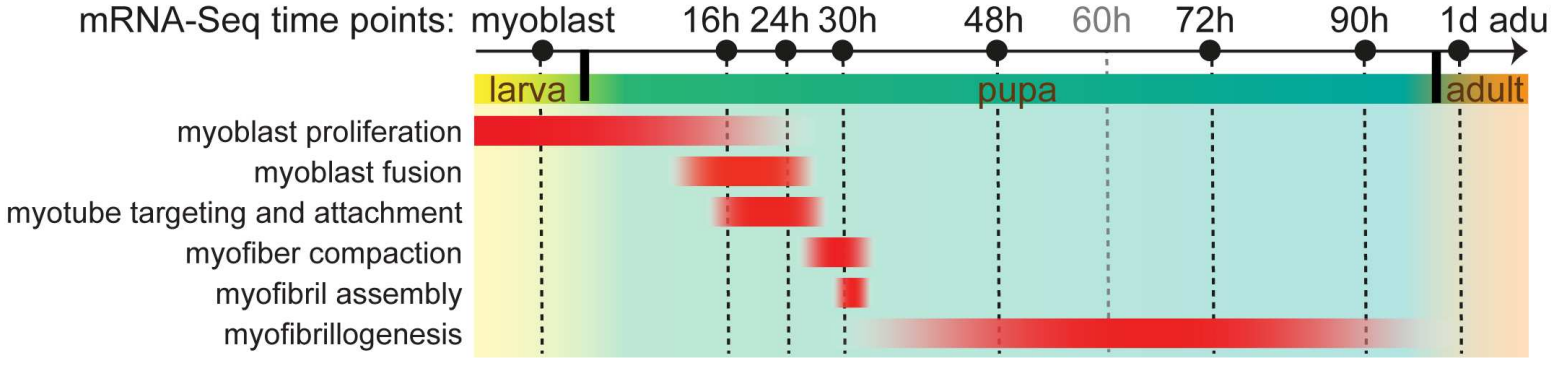

Spletter *et al.*, Figure 2

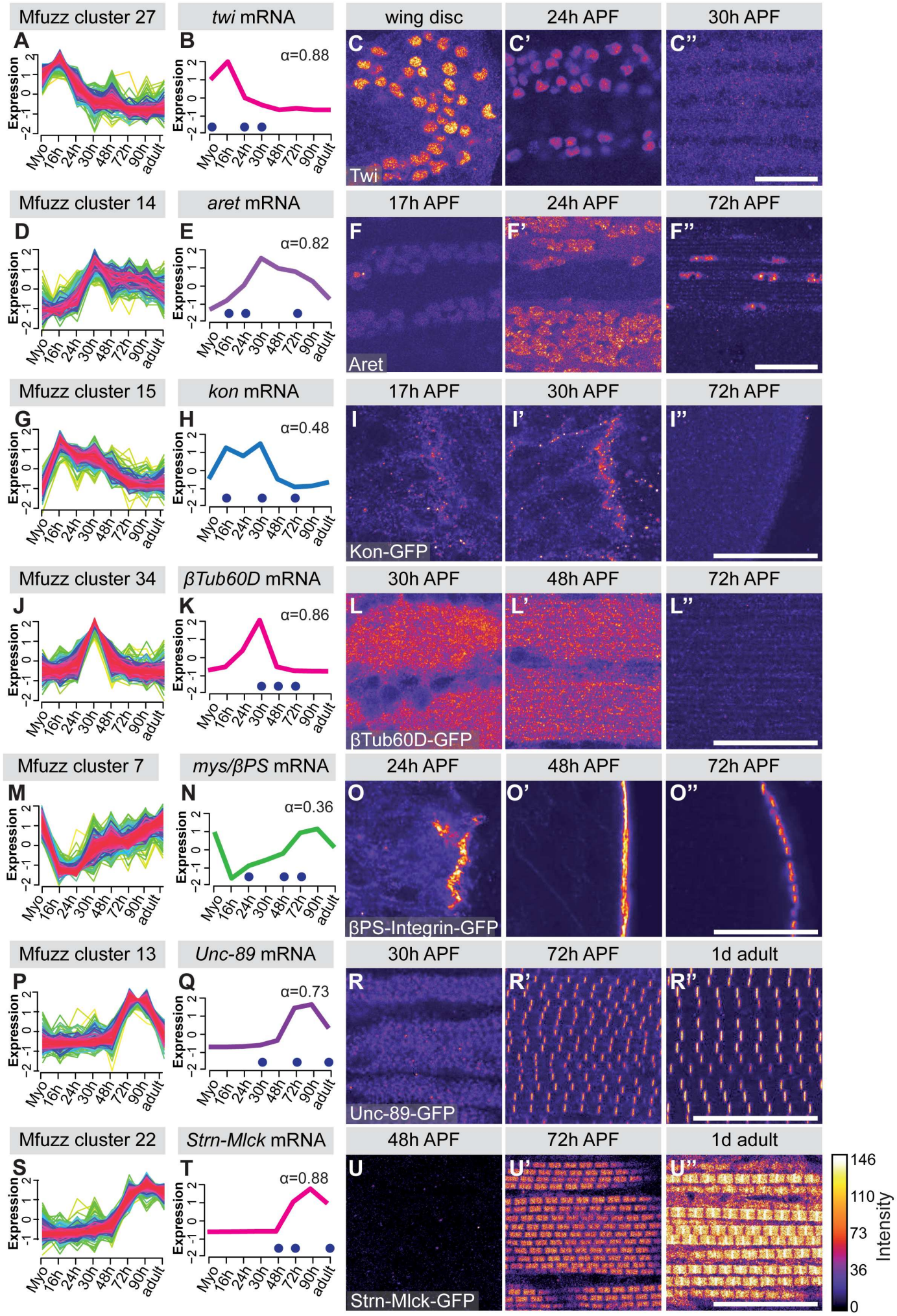

Spletter *et al.*, Figure 2 - Supplement 1

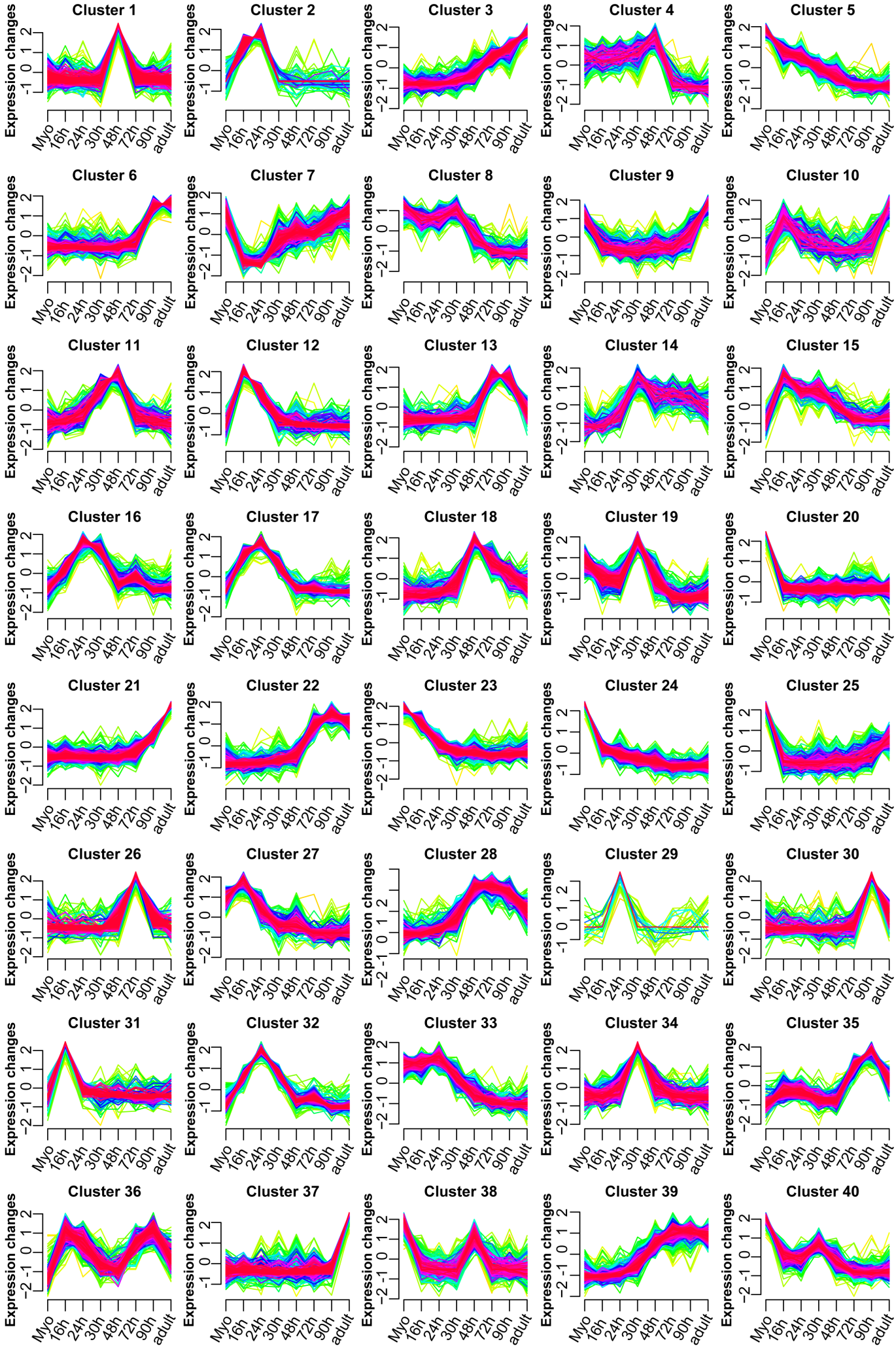

Spletter *et al.*, Figure 2 - Supplement 2

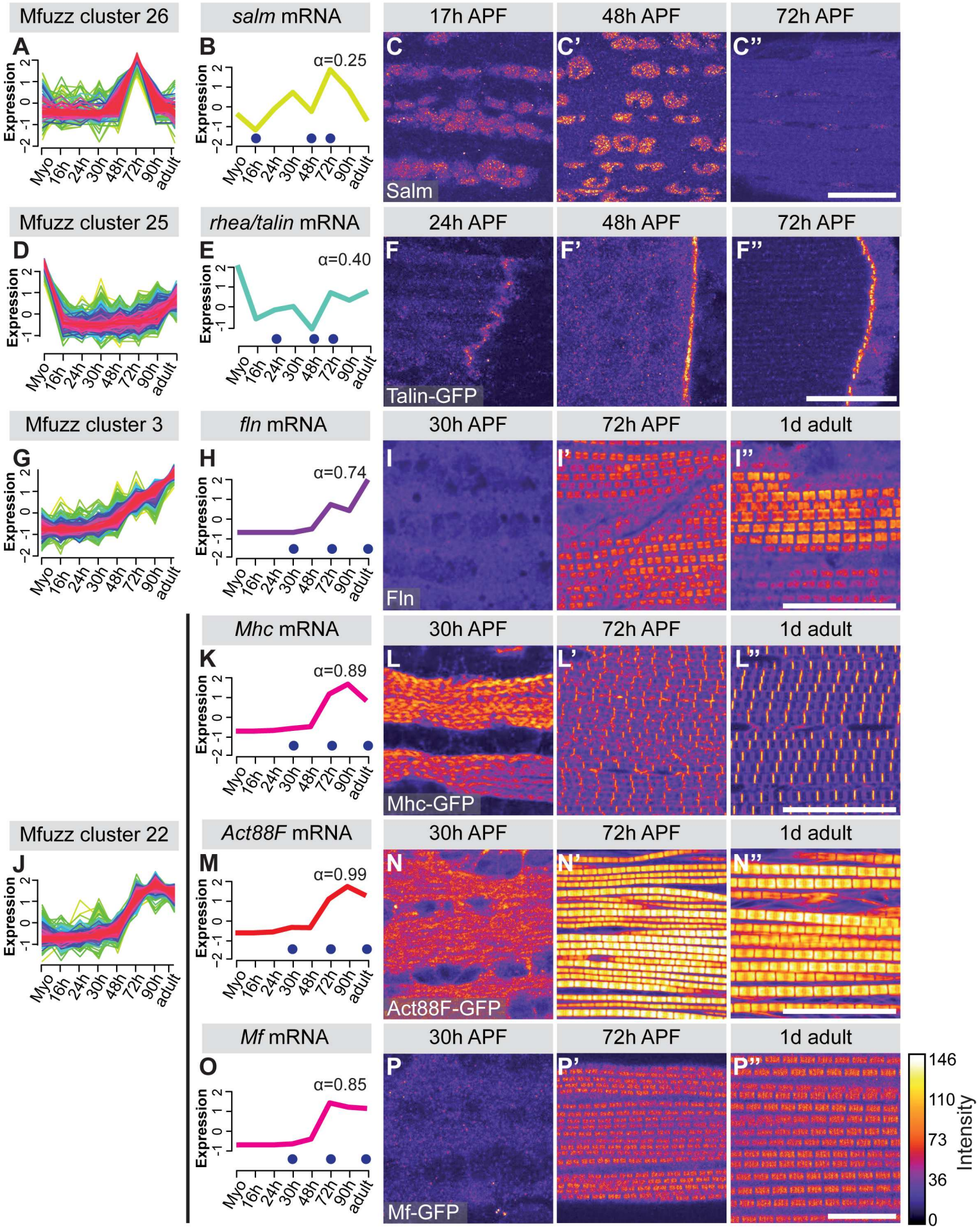

Spletter *et al.*, Figure 3

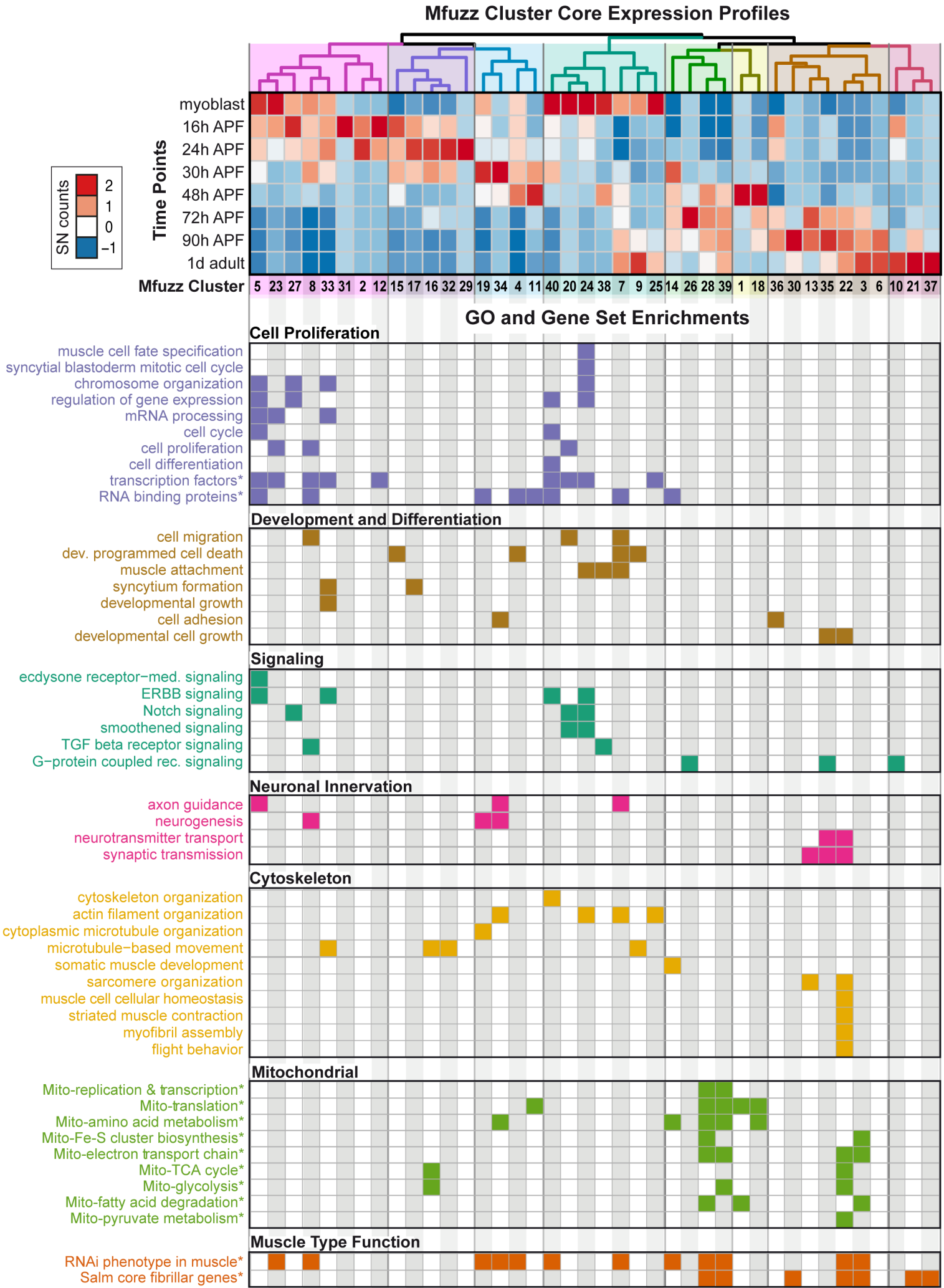

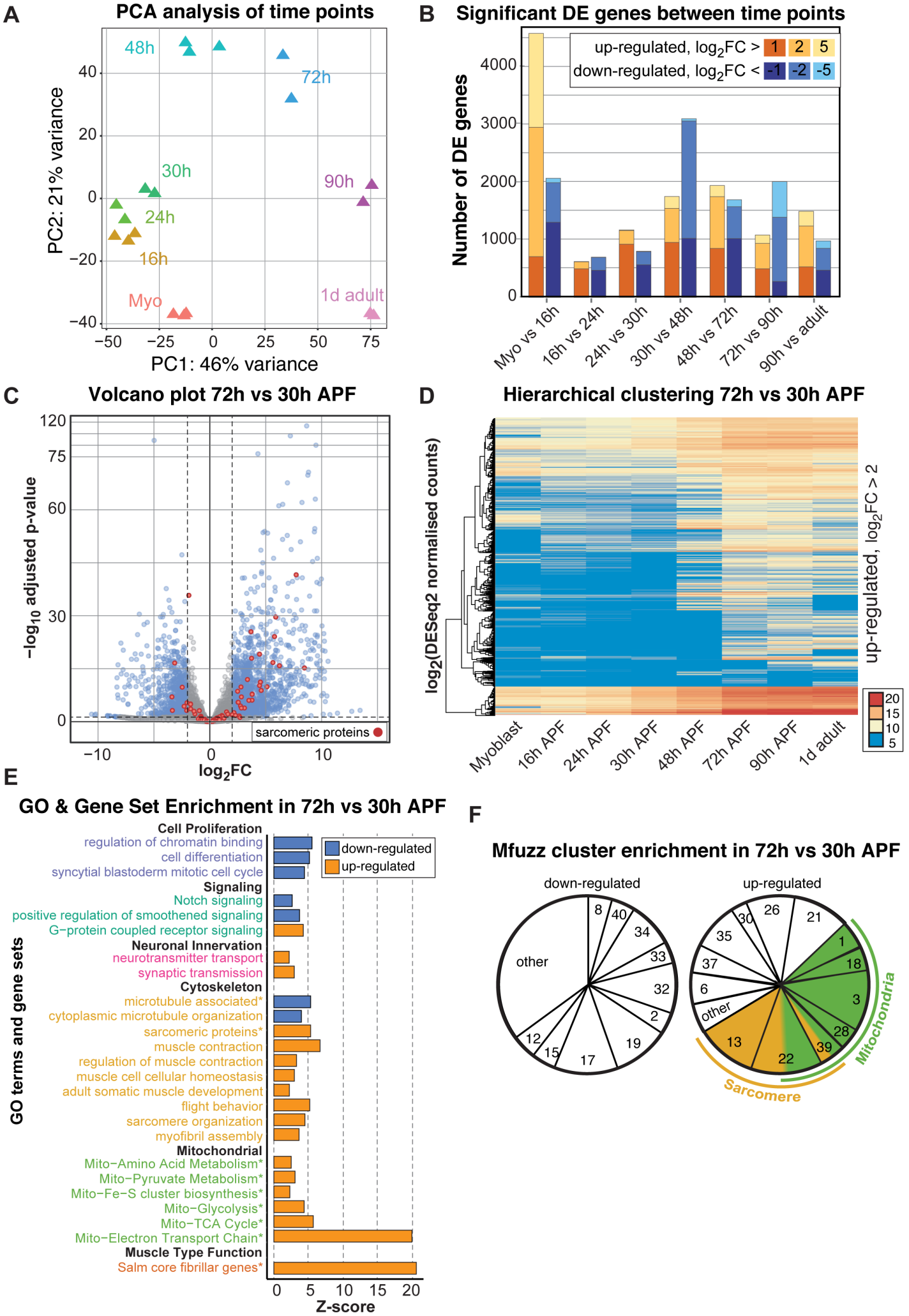
A
PCA analysis of time points
48h
72h
30h
90h
24h
16h
Myo
1d adult
PC2: 21% variance
PC1: 46% variance
B
Significant DE genes between time points
up-regulated, log2FC > 1 2 5
down-regulated, log2FC < -1 -2 -5
Number of DE genes
Myo vs 16h
16h vs 24h
24h vs 30h
30h vs 48h
48h vs 72h
72h vs 90h
90h vs adult
C
Volcano plot 72h vs 30h APF
−log10 adjusted p-value
log2FC
sarcomeric proteins
D
Hierarchical clustering 72h vs 30h APF
log2(DESeq2 normalised counts)
up-regulated, log2FC > 2
Myoblast
16h APF
24h APF
30h APF
48h APF
72h APF
90h APF
1d adult
E
GO & Gene Set Enrichment in 72h vs 30h APF
GO terms and gene sets
Cell Proliferation
regulation of chromatin binding
cell differentiation
syncytial blastoderm mitotic cell cycle
Signaling
Notch signaling
positive regulation of smoothened signaling
G−protein coupled receptor signaling
Neuronal Innervation
neurotransmitter transport
synaptic transmission
Cytoskeleton
microtubule associated*
cytoplasmic microtubule organization
sarcomeric proteins*
muscle contraction
regulation of muscle contraction
muscle cell cellular homeostasis
adult somatic muscle development
flight behavior
sarcomere organization
myofibril assembly
Mitochondrial
Mito−Amino Acid Metabolism*
Mito−Pyruvate Metabolism*
Mito−Fe−S cluster biosynthesis*
Mito−Glycolysis*
Mito−TCA Cycle*
Mito−Electron Transport Chain*
Muscle Type Function
Salm core fibrillar genes*
down-regulated
up-regulated
Z-score
F
Mfuzz cluster enrichment in 72h vs 30h APF
down-regulated
up-regulated
other
Mitochondria
Sarcomere

Spletter *et al.*, Figure 4 - Supplement 1

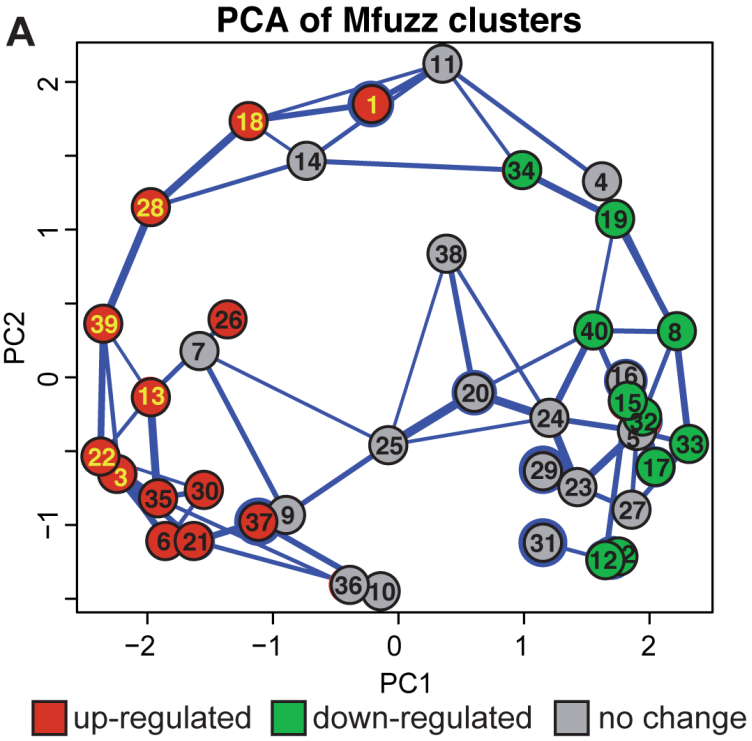

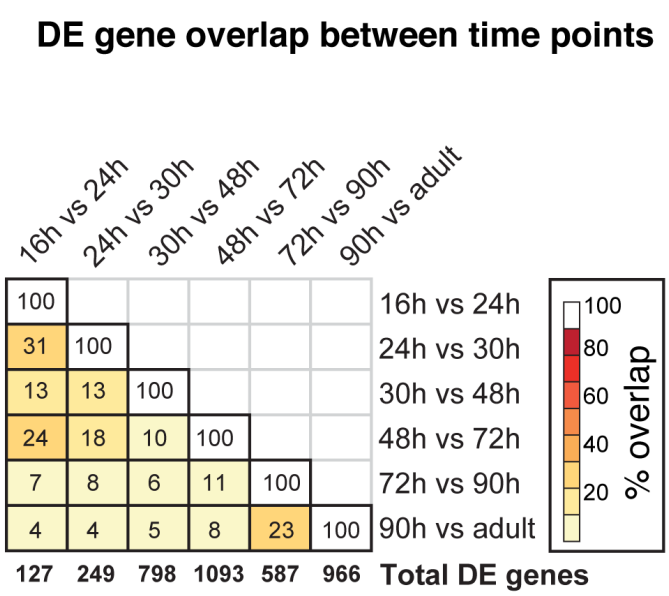

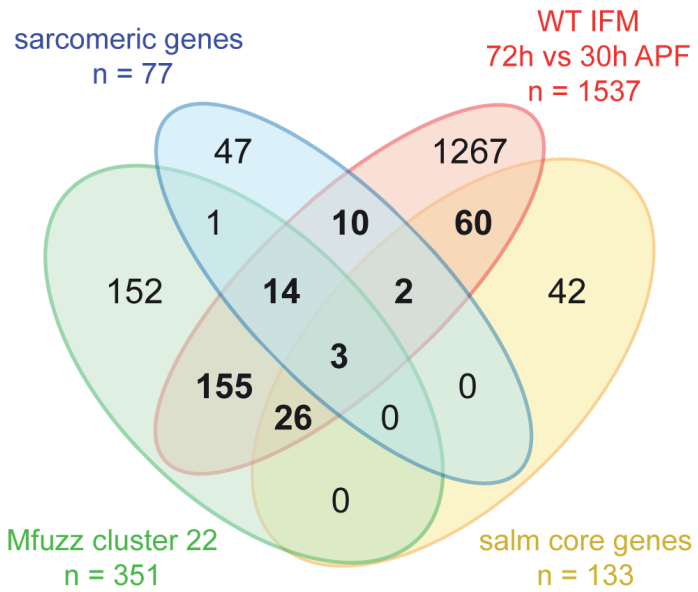

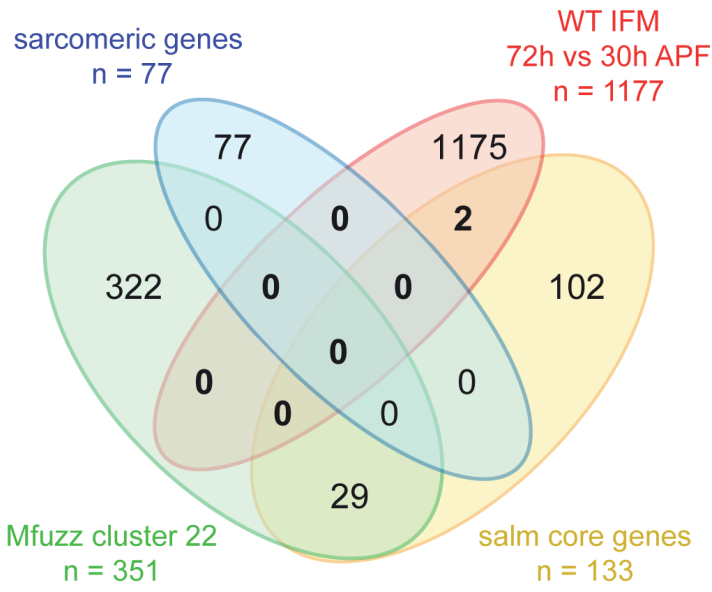

Spletter *et al.*, Figure 5

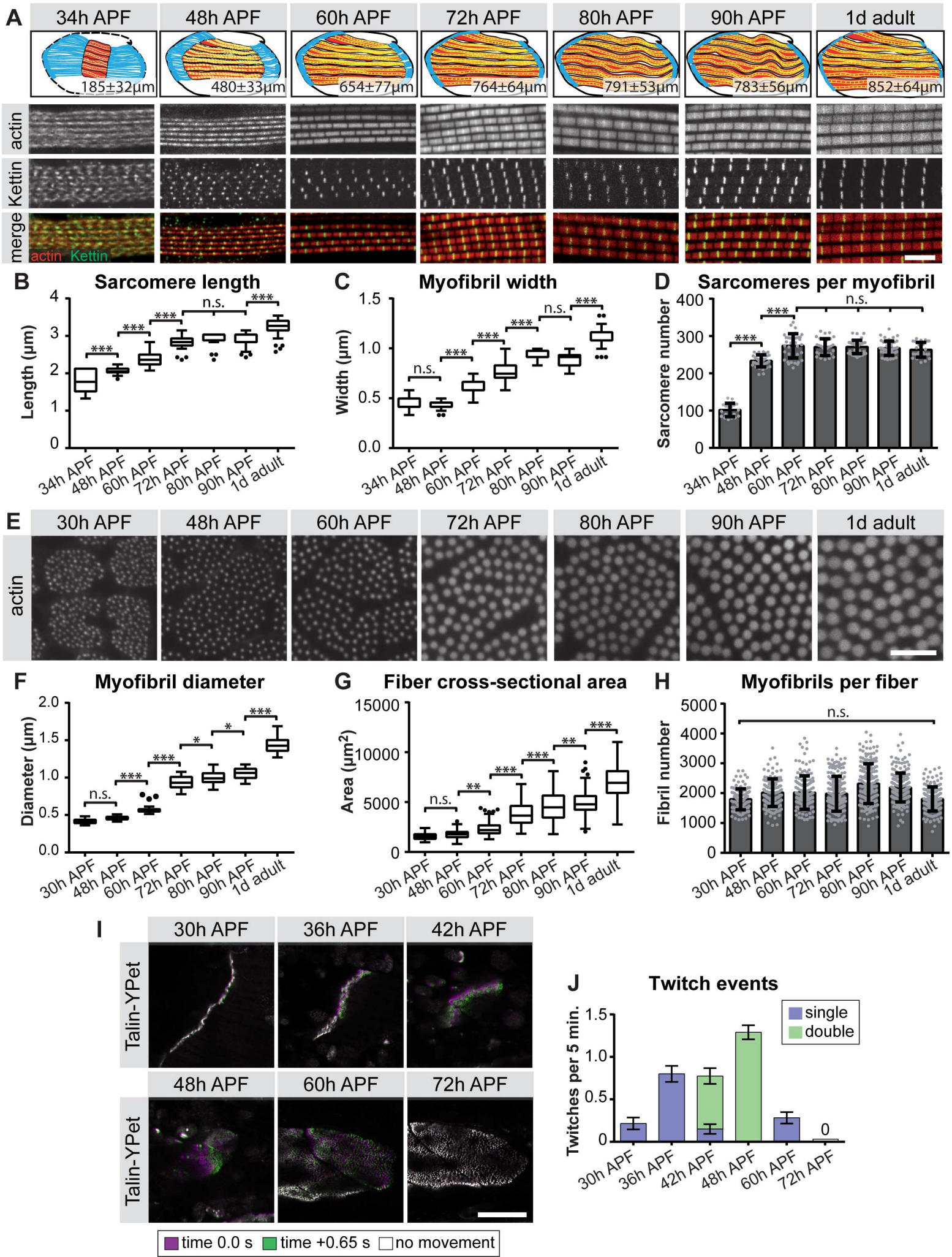

Spletter *et al.*, Figure 5- Supplement 1

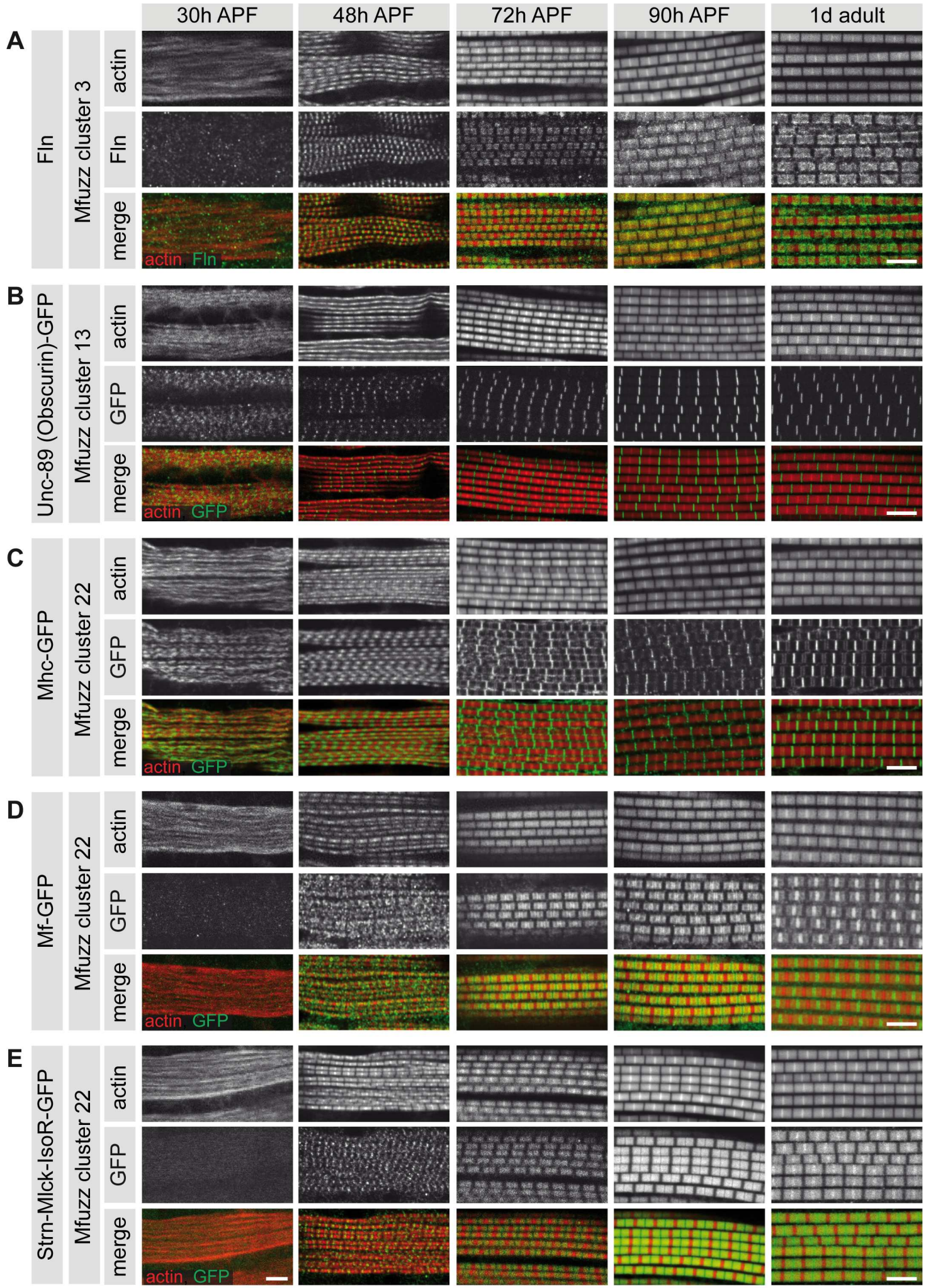

Spletter *et al.*, Figure 6

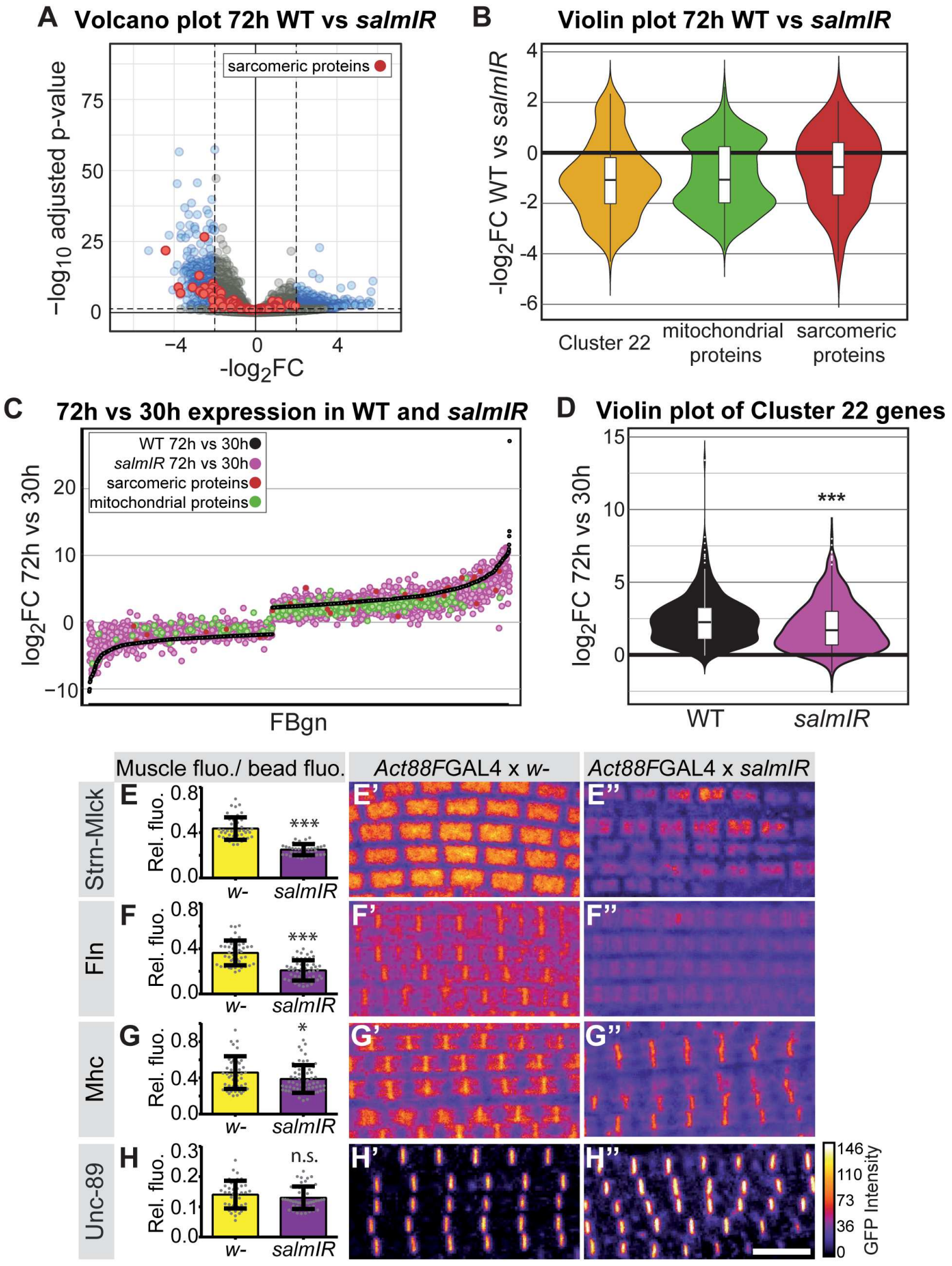

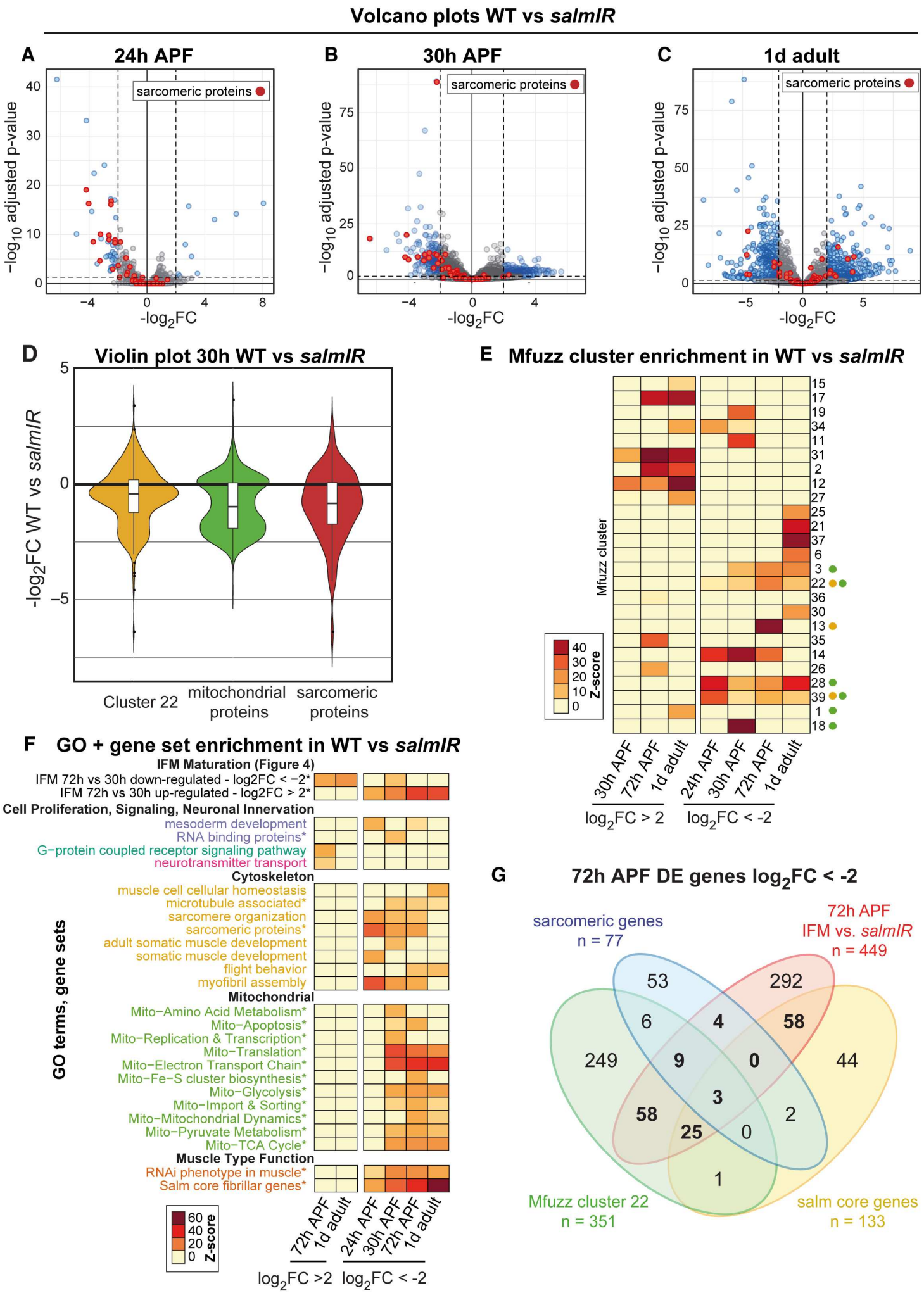
Volcano plots WT vs salmIR
A
24h APF
B
30h APF
C
1d adult
sarcomeric proteins
−log10 adjusted p-value
-log2FC
D
Violin plot 30h WT vs salmIR
-log2FC WT vs salmIR
Cluster 22
mitochondrial proteins
sarcomeric proteins
E
Mfuzz cluster enrichment in WT vs salmIR
Mfuzz cluster
Z-score
30h APF
72h APF
1d adult
24h APF
log2FC > 2
log2FC < -2
F
GO + gene set enrichment in WT vs salmIR
IFM Maturation (Figure 4)
IFM 72h vs 30h down-regulated - log2FC < −2*
IFM 72h vs 30h up-regulated - log2FC > 2*
Cell Proliferation, Signaling, Neuronal Innervation
mesoderm development
RNA binding proteins*
G−protein coupled receptor signaling pathway
neurotransmitter transport
Cytoskeleton
muscle cell cellular homeostasis
microtubule associated*
sarcomere organization
sarcomeric proteins*
adult somatic muscle development
somatic muscle development
flight behavior
myofibril assembly
Mitochondrial
Mito−Amino Acid Metabolism*
Mito−Apoptosis*
Mito−Replication & Transcription*
Mito−Translation*
Mito−Electron Transport Chain*
Mito−Fe−S cluster biosynthesis*
Mito−Glycolysis*
Mito−Import & Sorting*
Mito−Mitochondrial Dynamics*
Mito−Pyruvate Metabolism*
Mito−TCA Cycle*
Muscle Type Function
RNAi phenotype in muscle*
Salm core fibrillar genes*
GO terms, gene sets
Z-score
72h APF
1d adult
24h APF
30h APF
72h APF
1d adult
log2FC >2
log2FC < -2
G
72h APF DE genes log2FC < -2
sarcomeric genes
n = 77
72h APF
IFM vs. salmIR
n = 449
Mfuzz cluster 22
n = 351
salm core genes
n = 133
53
292
6
4
58
249
9
0
44
3
58
2
25
0
1

Spletter *et al*., Figure 6 - Supplement 2

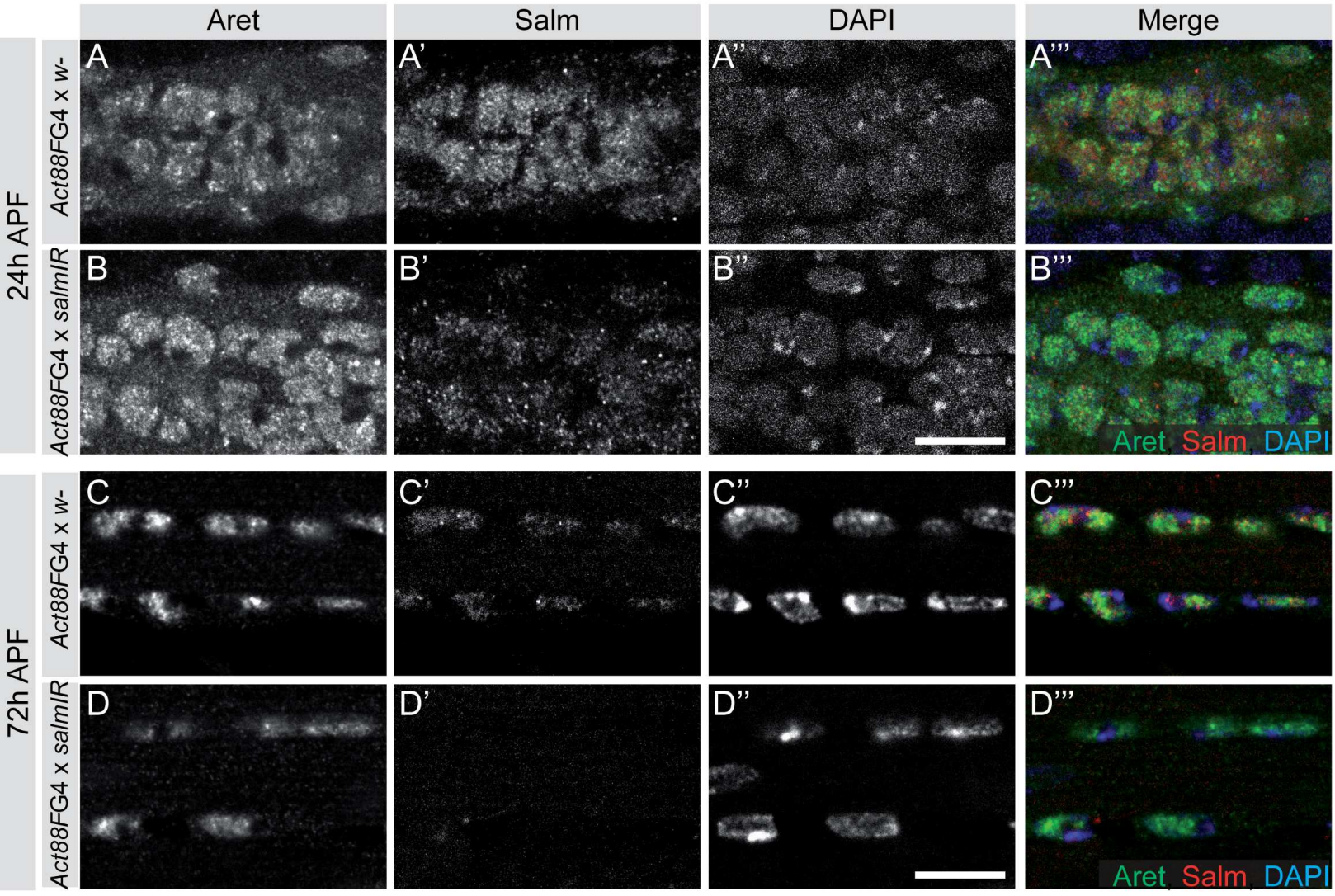

Spletter *et al*., Figure 6 - Supplement 3

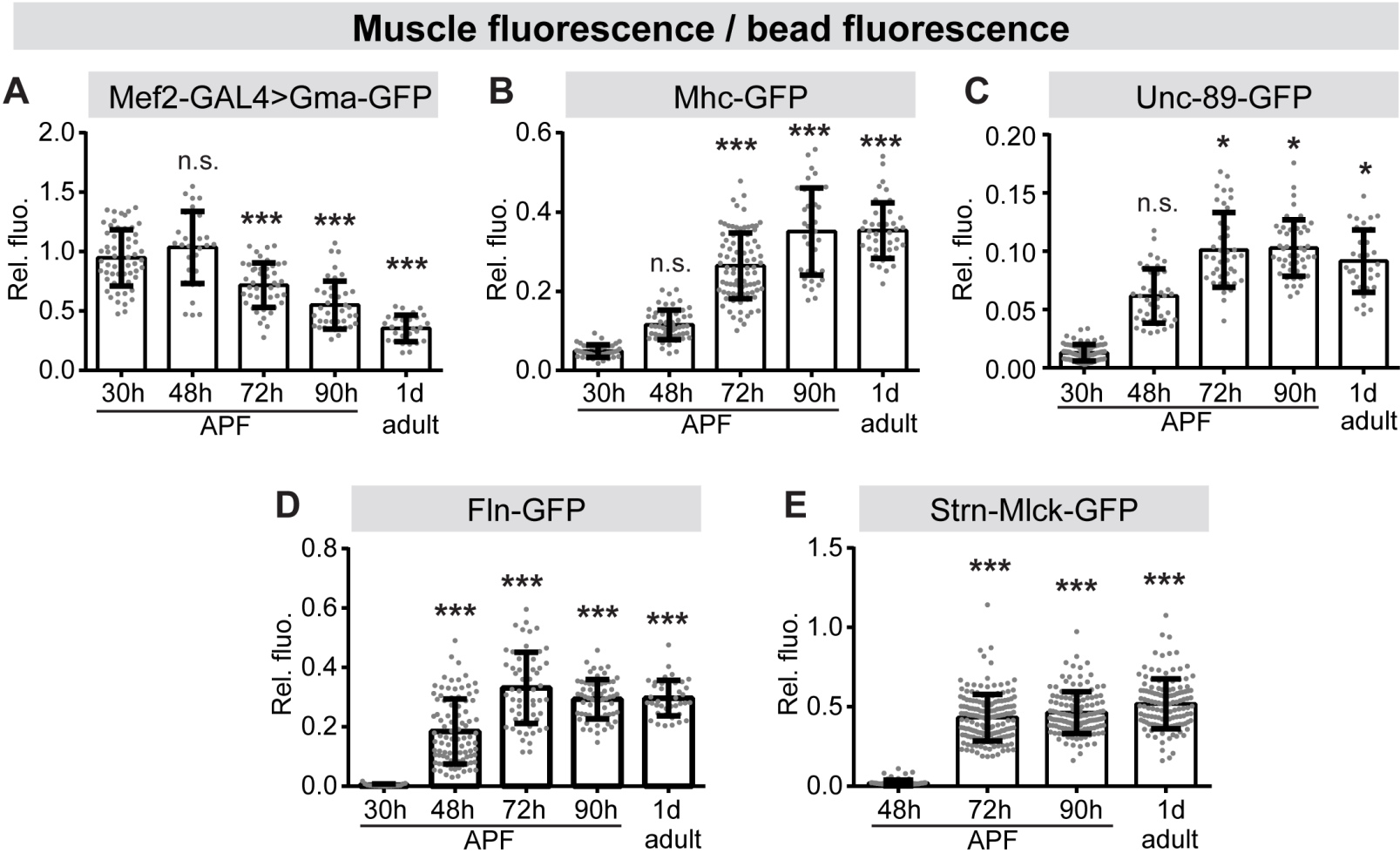

Spletter *et al.*, Figure 7

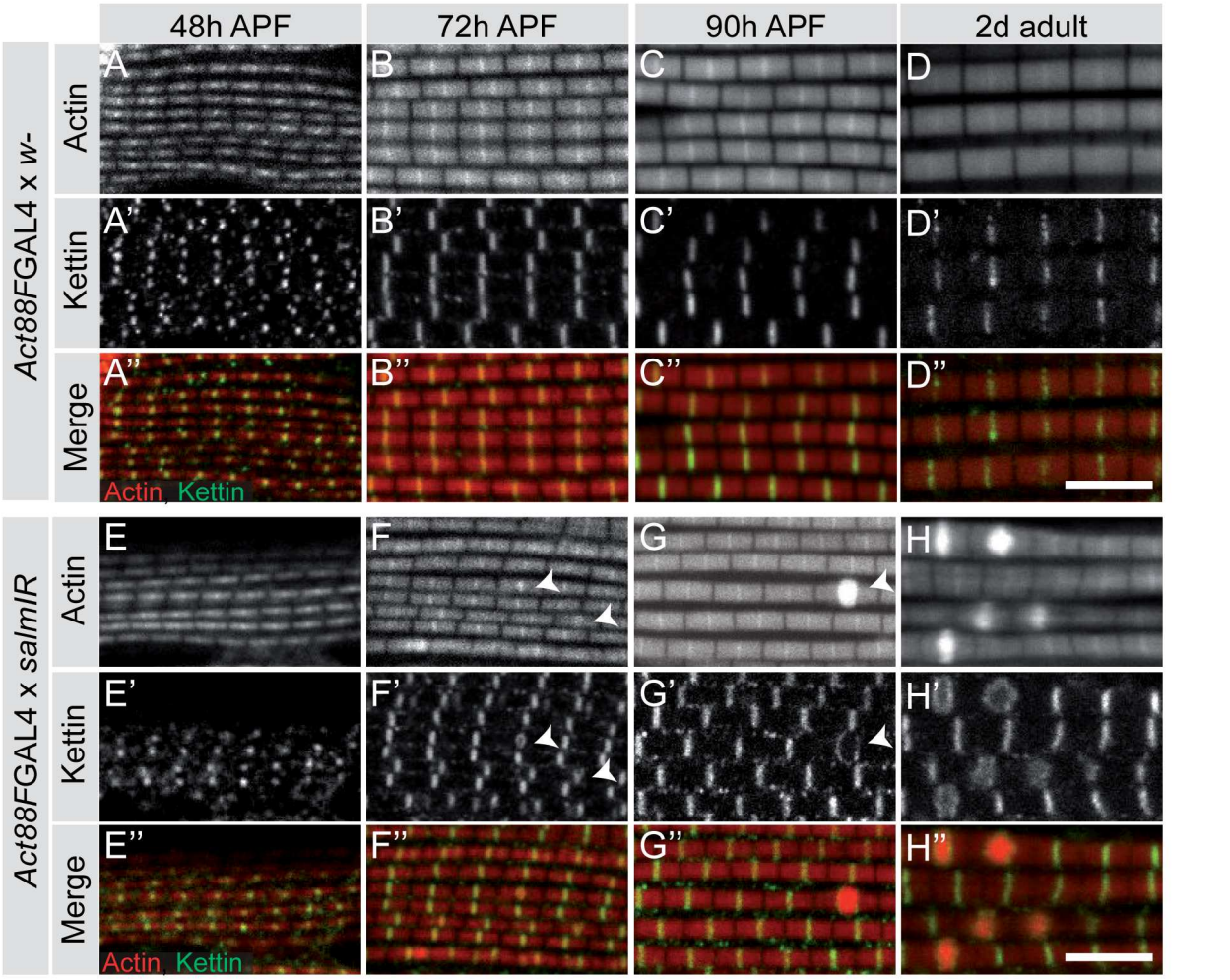

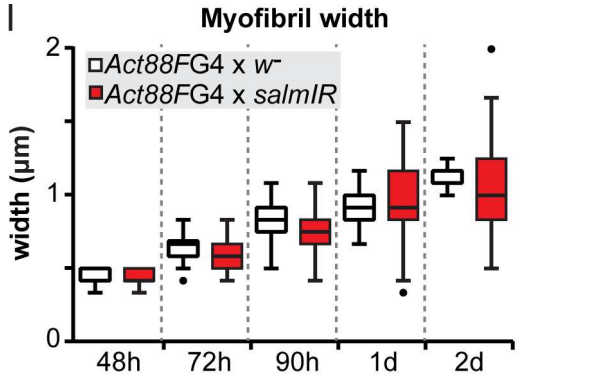

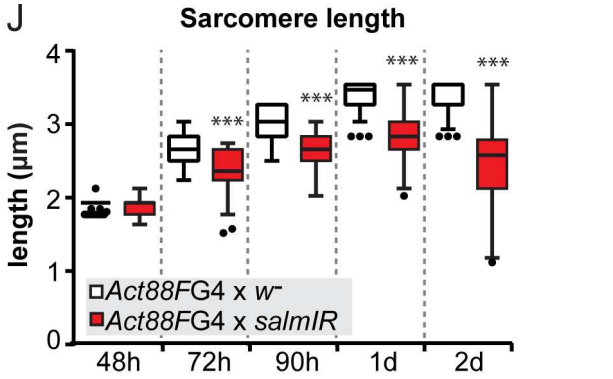

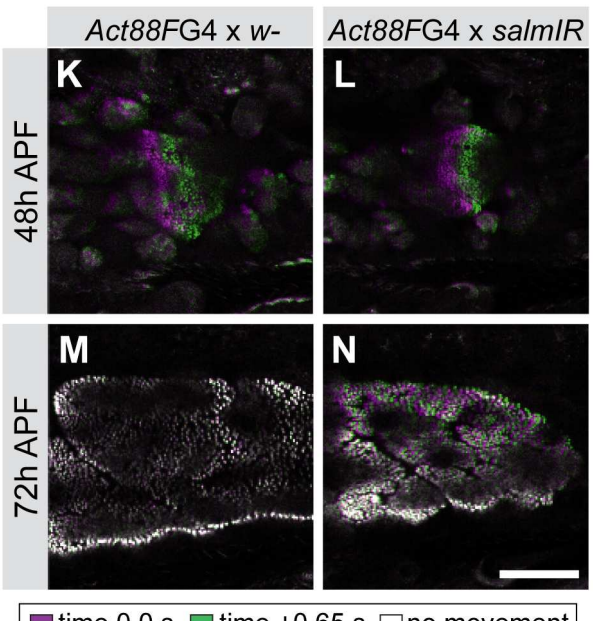

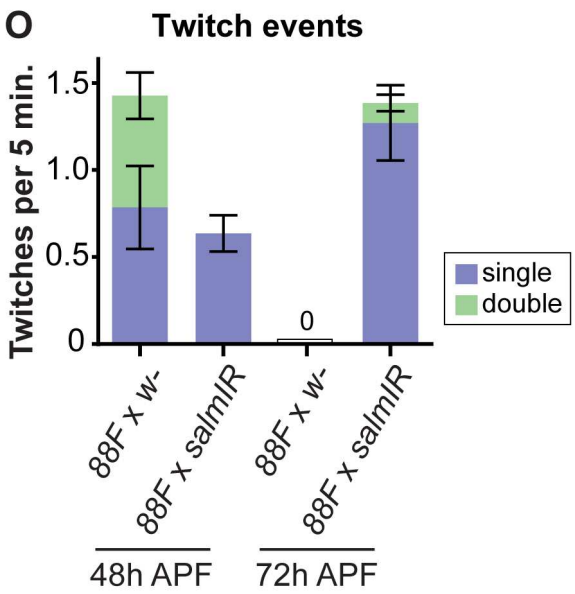

Spletter *et al.*, Figure 7 - Supplement 1

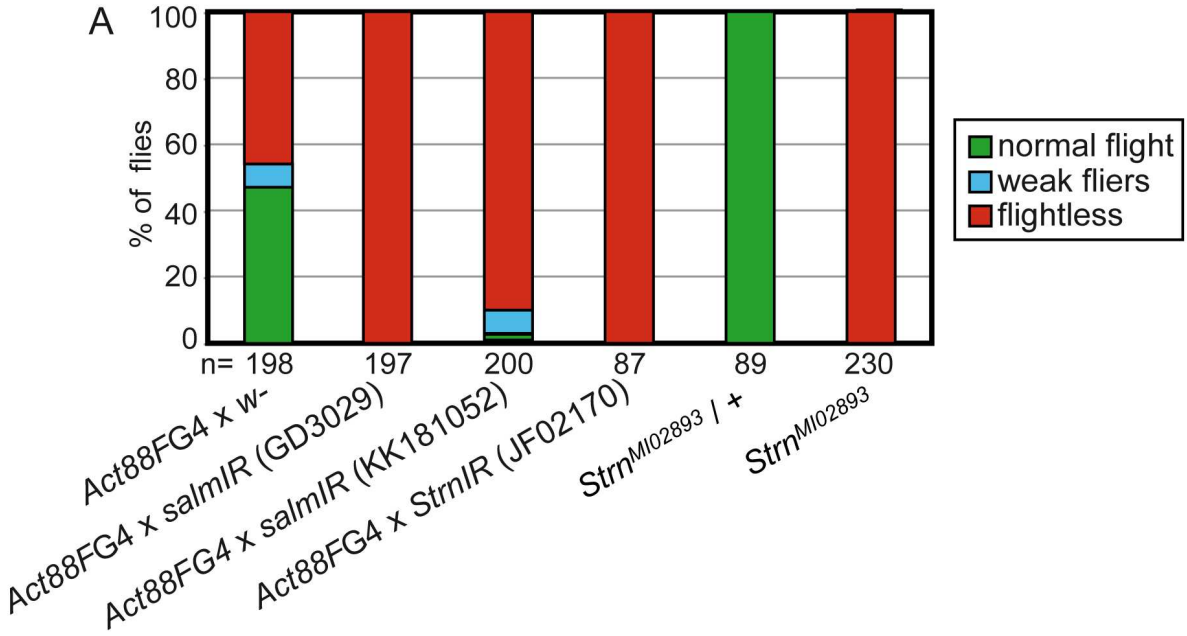

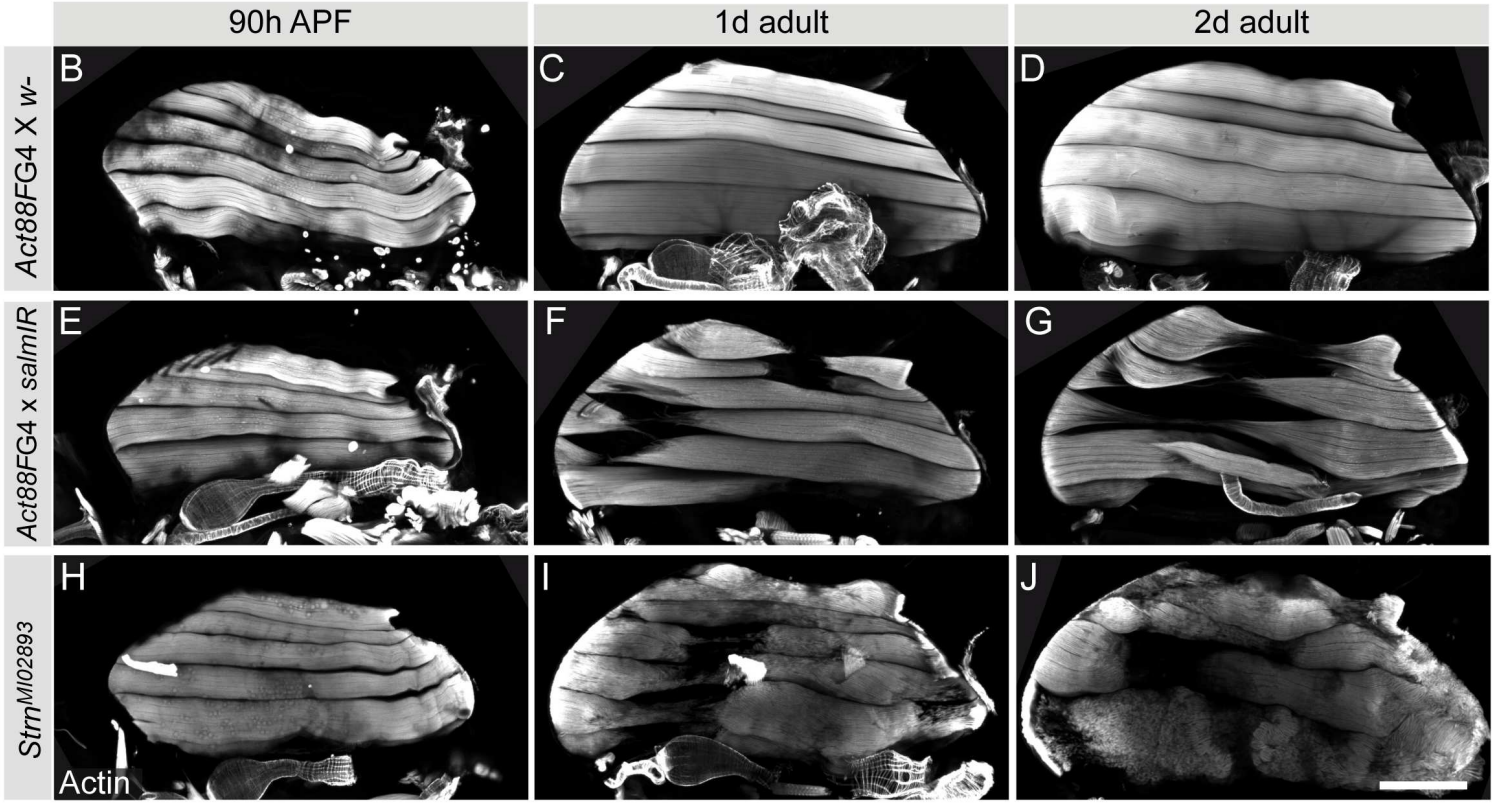

Spletter *et al.*, Figure 8

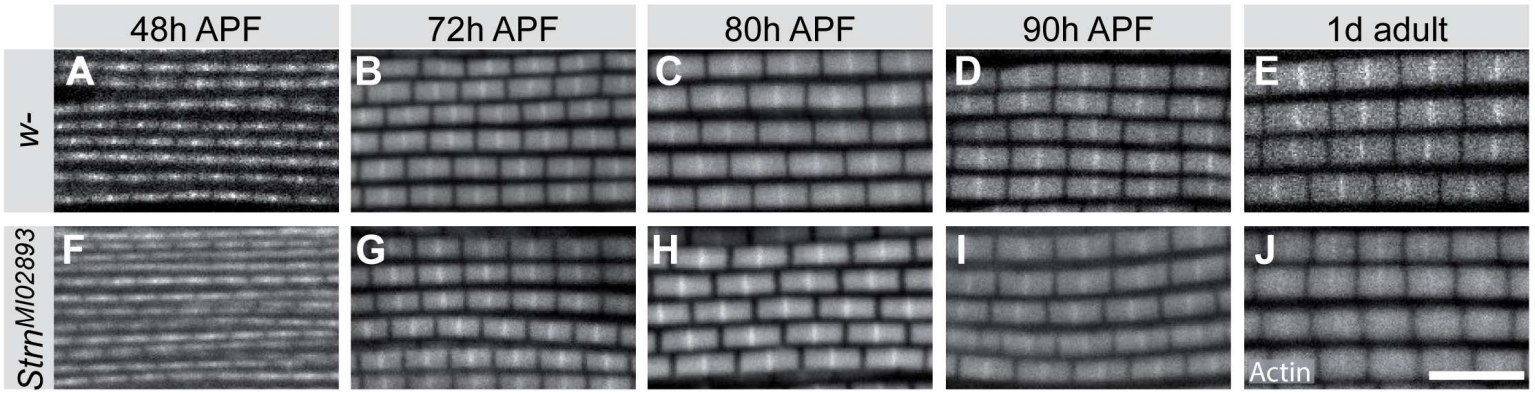

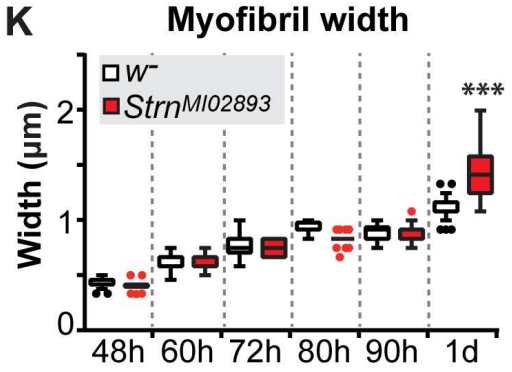

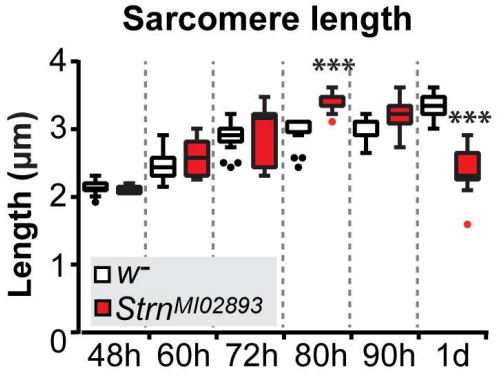

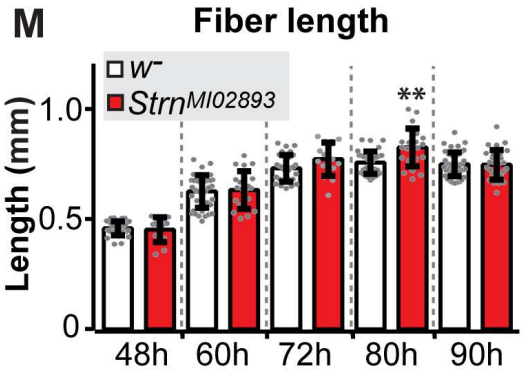

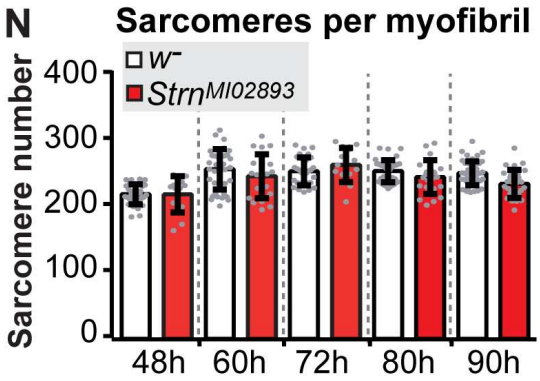

Spletter et al., Figure 9